ARTICLE

doi:10.1038/nature23282

Hypothalamic stem cells control ageing speed partly through exosomal miRNAs

Yalin Zhang[1]*, Min Soo Kim[1]*, Baosen Jia[1]*, Jingqi Yan[1]*, Juan Pablo Zuniga-Hertz[1], Cheng Han[1] & Dongsheng Cai[1]

It has been proposed that the hypothalamus helps to control ageing, but the mechanisms responsible remain unclear. Here we develop several mouse models in which hypothalamic stem/progenitor cells that co-express Sox2 and Bmi1 are ablated, as we observed that ageing in mice started with a substantial loss of these hypothalamic cells. Each mouse model consistently displayed acceleration of ageing-like physiological changes or a shortened lifespan. Conversely, ageing retardation and lifespan extension were achieved in mid-aged mice that were locally implanted with healthy hypothalamic stem/progenitor cells that had been genetically engineered to survive in the ageing-related hypothalamic inflammatory microenvironment. Mechanistically, hypothalamic stem/progenitor cells contributed greatly to exosomal microRNAs (miRNAs) in the cerebrospinal fluid, and these exosomal miRNAs declined during ageing, whereas central treatment with healthy hypothalamic stem/progenitor cell-secreted exosomes led to the slowing of ageing. In conclusion, ageing speed is substantially controlled by hypothalamic stem cells, partially through the release of exosomal miRNAs.

Although the nervous system clearly has a role in ageing[1–6], and research has demonstrated that the hypothalamus is particularly important[5–8], the cellular mechanism responsible for ageing is still unknown. It has been shown that adult neural stem/progenitor cells (NSCs) reside in a few brain regions that mediate local neurogenesis and therefore several aspects of brain functioning[9–13]. Studies on adult neurogenesis have focused on the hippocampus and the subventricular zone of the lateral ventricle in the brain[9–13]. Decreased neurogenesis in these regions often correlates with the advent of related ageing-associated disorders[10,14–18]. More recently, it has been shown that adult NSCs are present in the hypothalamus[19–21], in particular in the mediobasal hypothalamic region (MBH), which is crucial for the neuroendocrine regulation of the physiological homeostasis of the whole body. We have previously shown that the hypothalamus has a programmatic role in causing systemic ageing[5]. In this context, we investigated whether these hypothalamic NSCs (htNSCs) might be mechanistically responsible for this process.

Ageing-associated htNSC loss

Sox2 is a nuclear transcription factor that is strongly expressed in NSCs and has often been used to label NSCs[22]. We have found that, in adult mice, Sox2 is expressed in a population of cells in the MBH and especially in the hypothalamic third-ventricle wall within the MBH[19]. To gain an insight into their relevance to ageing, we comparatively examined these hypothalamic cells during ageing. Together with Sox2, we analysed the Polycomb complex protein Bmi1 (BMI1 in humans (B lymphoma Moloney murine leukaemia virus integration site 1 homologue))—a nuclear protein that is essential for self-renewal of NSCs and haematopoietic stem cells[23]. As shown in Fig. 1a, cells co-expressing Sox2 and Bmi1 were found to be densely present in the hypothalamic third-ventricle wall, whereas they were sporadically present in the MBH parenchyma of young mice. These cells gradually diminished with increased age, starting from the bottom part of the MBH of the hypothalamic third-ventricle wall in early- to mid-aged mice (11–16 months old) and becoming almost entirely lost in aged mice (22 months and older). We also examined nestin, which, although it is not NSC specific, is known to be strongly expressed in NSCs and their offspring progenitors[20,24,25]. To focus on the hypothalamic third-ventricle wall, we confirmed that nestin$^+$ cells in this region greatly decreased with age (Fig. 1b). In addition, because Musashi1 and Cxcr4 were also reported as NSC biomarkers[24,26], we examined both of these markers and found that the number of cells that were positive for Musashi1 and Cxcr4 in the hypothalamic third-ventricle wall decreased markedly during ageing. Moreover, through BrdU tracking, we confirmed that BrdU$^+$ cells were present in the hypothalamic third-ventricle wall of young mice, but were barely detected in this region in mid-aged mice (data not shown). Overall, the time course of age-dependent loss of htNSCs correlated well with ageing-related physiological declines (Extended Data Fig. 1), leading us to investigate whether the loss of these cells could be causally important for ageing.

Ageing acceleration due to htNSC loss

Because the hypothalamic third-ventricle wall is the area that sensitively undergoes loss of NSCs, we mimicked this change by experimentally ablating NSCs in this region. To do so, we adopted the approach of viral injection into the hypothalamic third ventricle, especially because the injected lentiviruses preferentially infected the third-ventricle surface, which contains the NSCs, but hardly penetrated the wall to infect the parenchyma (Extended Data Fig. 2a). Also, injected lentiviruses did not travel to distant regions, such as the lateral ventricle (Extended Data Fig. 2a). We ablated htNSCs by injection of lentiviruses that expressed herpes simplex virus thymidine kinase-1 (Hsv-TK1) controlled by a Sox2 promoter and by subsequently applying Ganciclovir (GCV), which is converted into a toxin by TK1. Therefore, TK1-expressing Sox2 cells in the hypothalamic third-ventricle wall were partially ablated. This treatment eventually led to a 70% loss of Sox2 cells in the hypothalamic third-ventricle wall of mice injected with both TK1 and GCV (hereafter TK1/GCV), without a major effect on parenchymal Sox2 cells or neurons (Fig. 1c–e). For this model, we separately analysed MBH neuronal subtypes, POMC and AgRP neurons, using POMC-Cre and AgRP-Cre mouse stains. TK1/GCV treatment did not decrease the number of these neurons (Extended Data Fig. 2b, c), and functionally optogenetic stimulation of each of these neuronal subtypes led to comparable feeding responses for TK1/GCV-injected mice and

[1]Department of Molecular Pharmacology, Diabetes Research Center, Institute of Aging, Albert Einstein College of Medicine, Bronx, New York 10461, USA.
*These authors contributed equally to this work.

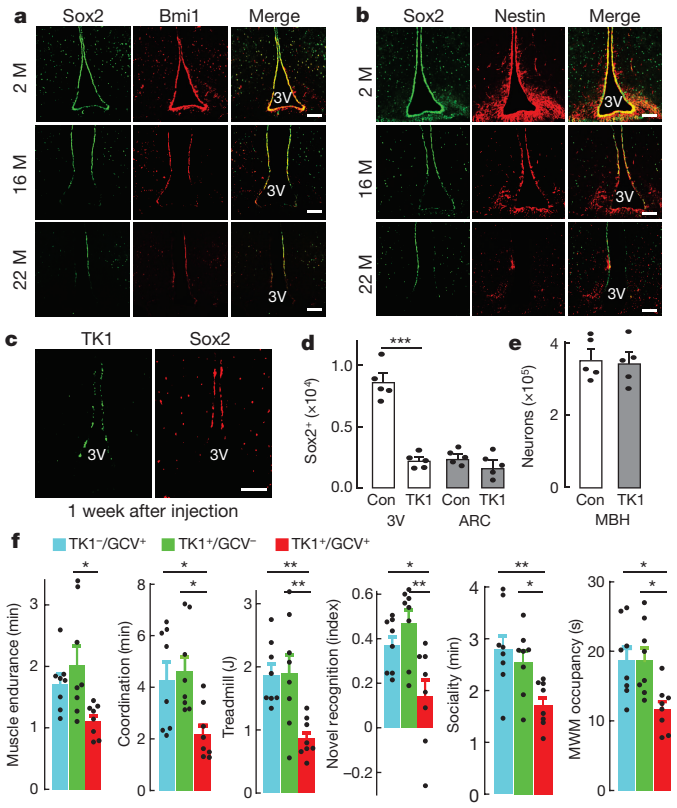

Figure 1 | Ageing-associated htNSC loss and its impact on ageing speed. **a**, **b**, Hypothalamic sections from male C57BL/6 mice at indicated months (M) of age were immunostained for Sox2 (**a**, **b**) and Bmi1 (**a**) or Nestin (**b**). 3V, third ventricle. **c**–**f**, Mid-aged C57BL/6 mice (15 months old) were injected in the hypothalamic third ventricle with Sox2-promoter-directed Hsv-TK1 (TK1) or control (Con) lentiviruses (**c**), followed by Ganciclovir (GCV) or vehicle treatment, and cell ablation (**d**, **e**) and physiology (**f**) three months after viral injection were examined. **d**, **e**, Number of $Sox2^+$ cells and $NeuN^+$ neurons in hypothalamic third-ventricle wall, arcuate nucleus (ARC) or MBH. MWM, Morris Water Maze (see Extended Data Fig. 2e). Images represent three independent experiments (**a**–**c**). Scale bars, 100 μm. $*P < 0.05$, $**P < 0.01$, $***P < 0.001$; two-tailed Student's *t*-test (**d**, **e**) or one-way ANOVA with Tukey's test (**f**); $n = 5$ mice (**d**, **e**) and $n = 8$ mice (**f**) per group. Data are mean ± s.e.m.

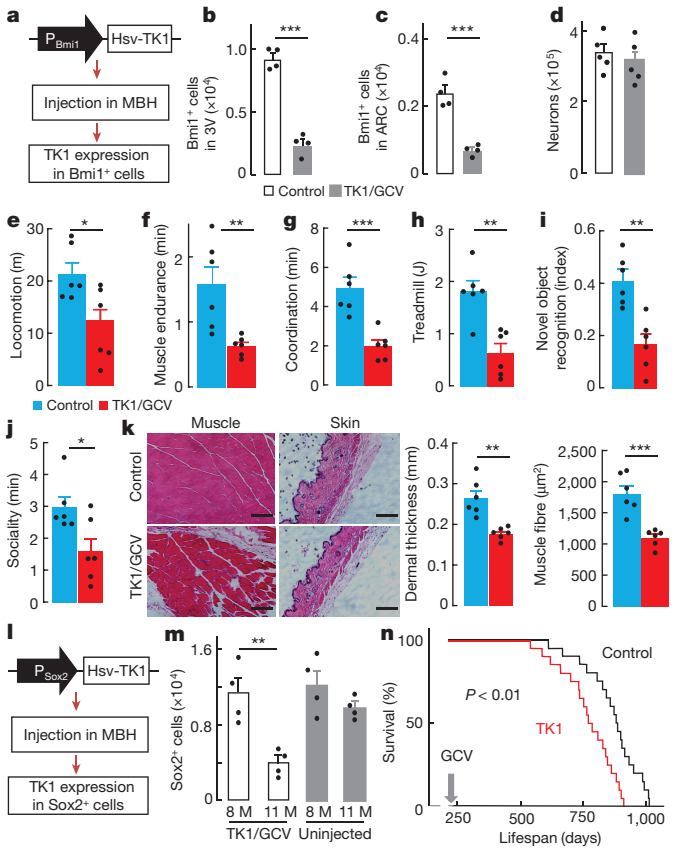

Figure 2 | Ageing acceleration and lifespan shortening due to htNSC loss. Mid-aged male C57BL/6 mice (15 months old) were bilaterally injected in the MBH with Bmi1-promoter-driven Hsv-TK1 (TK1) or control lentiviruses, followed by GCV or vehicle treatment. **a**, Diagram of TK1 lentivirus and injection. **b**–**d**, $Bmi1^+$ cells in the hypothalamic third-ventricle wall (**b**) and ARC (**c**), and $NeuN^+$ neurons in the MBH (**d**) at three months after viral injection. **e**–**k**, At around 3–4 months after viral injection, the $TK1^+/GCV^+$ group (labelled as TK1/GCV) was compared to control groups (data derived from the $TK1^+/GCV^-$ group, but also representative of $TK1^-/GCV^+$ and $TK1^-/GCV^-$ groups) for physiology (**e**–**j**) and histology (**k**). Images represent two independent experiments. Scale bars, 100 μm. **l**–**n**, Male C57BL/6 mice (8 months old) were bilaterally injected in the MBH with Sox2-promoter-driven Hsv-TK1 (TK1) or control lentiviruses, followed by GCV treatment. **l**, Diagram of TK1 lentivirus and injection in the MBH. **m**, $Sox2^+$ cells in MBH parenchyma and hypothalamic third-ventricle wall of mice injected with TK1/GCV (age-matched uninjected mice are included as a reference). **n**, Lifespan follow-up. $*P < 0.05$, $**P < 0.01$, $***P < 0.001$; two-tailed Student's *t*-test (**b**–**k**), two-way ANOVA with post hoc test (**m**), log-rank (Mantel–Cox) test (**n**); $n = 4$ mice (**b**, **c**, **m**), $n = 5$ mice (**d**) and $n = 6$ mice (**e**–**k**) per group, and $n = 19$ mice for control and $n = 20$ mice for TK1 (**n**). Data are mean ± s.e.m.

controls (Extended Data Fig. 2d). To study ageing-related physiology, the TK1/GCV model and various control groups were used at a mid-age. Compared to control groups over an approximately 3–4-month follow-up, TK1/GCV mice displayed accelerated decreases in muscle endurance, coordination, treadmill performance, sociality and novel object recognition (Fig. 1f). Analysis of the performance in the Morris water maze test showed that TK1/GCV-injected mice manifested a cognitive decline more than the controls did (Fig. 1f and Extended Data Fig. 2e). In comparison with the regular speed of ageing progression in wild-type C57BL/6 mice (Extended Data Fig. 1), all of these physiological changes in TK1/GCV-injected mice reflected an acceleration in ageing.

In parallel, we used an alternative cell-ablation method to test whether it could reproduce the pro-ageing phenotype of the TK1/GCV model. A previous study[27] has shown that the expression of inducible diphtheria toxin receptor (DTR) followed by the administration of diphtheria toxin led to cell ablation in these mice. Therefore, we generated lentiviruses that expressed DTR controlled by the Sox2 promoter, as indicated in Extended Data Figure 3a, b. We then injected this DTR lentivirus or a control lentivirus into the hypothalamic third ventricle of mid-aged mice, followed by diphtheria toxin administration to activate DTR. This approach resulted in a significant ablation of Sox2 cells in the hypothalamic third-ventricle wall, while MBH parenchymal cells were barely affected (Extended Data Fig. 3c, d). Indeed, DTR and diphtheria toxin treatment gradually led to accelerated physiological declines (Extended Data Fig. 3e), similar to what was seen in the TK1/GCV model described above.

Additional experiments were performed through intra-MBH viral injection, which led to the restriction of htNSC ablation to the MBH part of the third-ventricle wall and the MBH parenchyma. Similar to the Sox2-promoter-based targeting in Figure 1, we used a Bmi1 promoter to direct TK1 expression. We delivered the TK1 or control lentiviruses bilaterally into the MBH of mid-aged mice (Fig. 2a), which led to a significant loss of NSCs in the MBH portion of the third-ventricle wall and the parenchyma (Fig. 2b, c), whereas the number of neurons in the MBH did not decrease (Fig. 2d). Compared to controls over a 3–4-month follow-up, TK1/GCV-injected mice clearly showed ageing-like physiological declines (Fig. 2e–h), cognitive impairment (Fig. 2i, j) and

histopathology (Fig. 2k). In addition, we set up a cohort of 8-month-old mice that were injected with TK1 or control lentiviruses for a lifespan follow-up. This model was based on Sox2-promoter-driven TK1 expression and MBH injection (Fig. 2l, m). As shown in Figure 2n, there was a significant decrease in the lifespan of TK1/GCV-treated mice compared to controls. Hence, results from these additional models consistently indicate that the MBH is essential for the role of htNSCs in controlling the speed of ageing.

Slowdown of ageing by implantation of IκBα–htNSCs

We simultaneously investigated whether htNSCs could be implanted into the MBH to slow down the progression of ageing. For the initial trial, we used a line of htNSCs derived from newborn mice that were labelled with GFP by lentiviral induction as has been described previously[19] and injected these cells into the MBH of mid-aged mice. However, these NSCs survived poorly after injection. This failure could be related to an inflammatory hypothalamic environment[5], as we have shown that hypothalamic inflammation is harmful for htNSCs[19]. Therefore, we asked whether inhibition of the inflammatory response in these cells might help to overcome this survival problem. To do so, we used htNSCs derived from newborn mice that stably expressed dominant-negative IκBα and GFP (IκBα-htNSCs). We have previously shown that these cells are resilient to NF-κB-mediated inflammation, compared to control htNSCs that stably expressed GFP (control-htNSCs)[19]. We implanted the same number of IκBα-htNSCs or control-htNSCs into the MBH of mid-aged mice. IκBα-htNSCs demonstrated a pronounced improvement in survival (Fig. 3a), showing that around 50% of grafted IκBα-htNSCs were alive, whereas few grafted control-htNSCs were found at two months after implantation. Then, we set up a group of mid-aged C57BL/6 mice that were bilaterally injected in the MBH with IκBα-htNSCs to study ageing-related physiology. For comparison, in addition to vehicle injection, a group of age-matched mice was injected with the same number of hypothalamic astrocytes. Hypothalamic astrocytes were derived from newborn mice, cultured and confirmed by immunostaining for the presence of the astrocyte marker S100B and the absence of NSC markers. In addition, we included mesenchymal stem cells (MSCs) as another type of comparison, because MSCs represent stem cells from a different embryonic origin. All cells were genetically labelled with GFP, and the same number of cells was bilaterally injected. Of note, astrocytes and MSCs were relatively insensitive to ageing-associated hypothalamic inflammation, because without genetic anti-inflammatory manipulation these cells survived to a level that was comparable to IκBα-htNSCs (Fig. 3b). Compared to vehicle controls, implanted IκBα-htNSCs led to a battery of systemic benefits, which were already recognizable at six weeks after implantation and continued to be more appreciable at four months after implantation (Fig. 3c). By contrast, no effects were identified after the implantation of astrocytes or MSCs (Fig. 3c). Independently, we generated separate groups of mid-aged mice injected in the MBH with IκBα-htNSCs for lifespan follow-up, while the control groups were injected with control-htNSCs or vehicle. Control-htNSCs did not induce a significant change in lifespan compared to vehicle control (data not shown), consistent with the fact that these cells did not survive long enough. By contrast, consistent with the anti-ageing effects (Fig. 3c), mice injected with IκBα-htNSCs demonstrated an increase in lifespan (Fig. 3d). To summarize, a local restoration of htNSCs in mid-aged mice can provide a substantial anti-ageing and longevity effect.

Endocrine secretion of exosomal miRNAs by htNSCs

As described above, the modulation of ageing by htNSCs, when ablated or implanted, was observable in a relatively short period (three to four months), therefore we reasoned that an endocrine function rather than neurogenesis of these cells was responsible. Considering that the pool of htNSCs is small, yet the effects on modulating of ageing are remarkable, we asked whether these cells might secrete substances that could have multifaceted functions. We considered exosomal miRNAs,

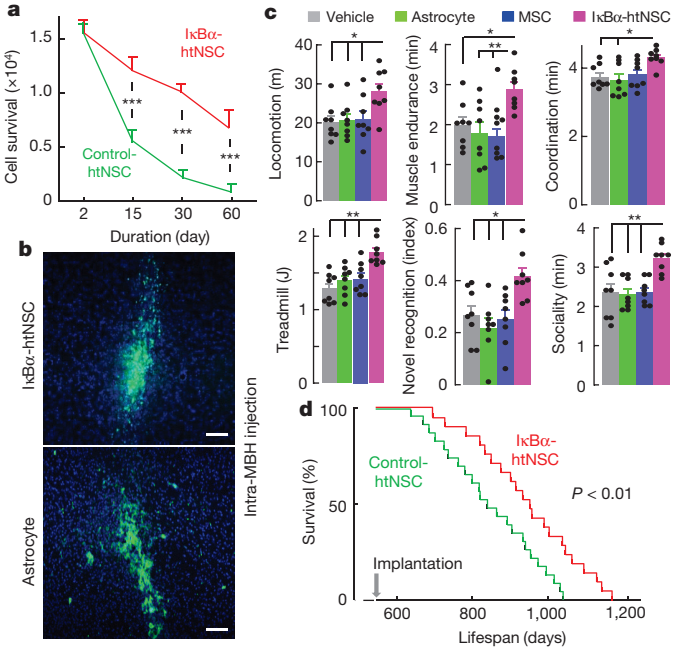

Figure 3 | Slowdown of ageing by hypothalamic implantation of IκBα-htNSCs. a, GFP-expressing IκBα-htNSCs or control-htNSCs were implanted bilaterally into the MBH of mid-aged C57BL/6 mice. Survival at indicated days after implantation was analysed. **b**, **c**, GFP-labelled IκBα-htNSCs, astrocytes (**b**) and MSCs (image not shown) were implanted into the MBH of 16-month-old male C57BL/6 mice and examined for GFP expression at one month after implantation (**b**) and ageing-related physiology at four months after implantation (**c**). Scale bars, 100 μm. **d**, IκBα-htNSCs or control-htNSCs were implanted bilaterally into the MBH of male C57BL/6 mice (18 months old) for lifespan follow-up. Images represent two independent experiments (**b**). $*P < 0.05$, $**P < 0.01$ (**a**, **c**); two-way ANOVA with post hoc test (**a**), one-way ANOVA with Tukey's test (**c**), log-rank (Mantel–Cox) test (**d**); $n = 4$ mice (**a**) and $n = 8$ mice (**c**) per group, and $n = 23$ mice for control-htNSCs and $n = 21$ mice for IκBα-htNSCs (**d**). Data are mean ± s.e.m.

because miRNAs have been linked to stem cell function[28,29] as well as to ageing[30]. Our prediction was supported by immunostaining for the exosomal protein CD81 and electron microscopic analysis, which showed that granule-like structures (Extended Data Fig. 4a) and multivesicular bodies (Extended Data Fig. 4b) were abundantly present in htNSCs, but were poorly detected in astrocytes from the same hypothalamus. Then, we isolated exosomes that were secreted from cultured htNSCs, as verified through a list of assays, including western blotting (Fig. 4a), flow cytometry (Extended Data Fig. 4c) and nanoparticle analysis (Fig. 4b and Extended Data Fig. 4d). The secreted exosomes that we isolated were also subjected by fractioning using density gradient ultracentrifugation or pull-down using the anti-CD81 antibody (Extended Data Fig. 5), both analyses confirmed that miRNAs were detected in the exosome fractions. Nanoparticle analysis was further used to compare exosomes secreted from htNSCs or other cells (Fig. 4b), showing that exosomes secreted from htNSCs were notably more abundant compared to exosomes secreted by astrocytes, GT1-7 cells and MSCs. Using the Qubit RNA assay to quantify exosomal RNA, we found that secreted exosomes of htNSCs contained a large amount of RNA. We analysed the miRNA in these secreted exosomes, showing that miRNA produced by htNSCs was more abundant than miRNA produced by hippocampal NSCs, and the production by htNSCs was approximately 100-fold higher than by hypothalamic astrocytes, GT1-7 cells and MSCs (Fig. 4c and Extended Data Fig. 6a, b). Subsequently, we profiled exosomal miRNAs secreted by these different cells using microarray affymetrix chips, showing that htNSCs were most strongly capable of the secretion of exosomal miRNAs (Fig. 4d).

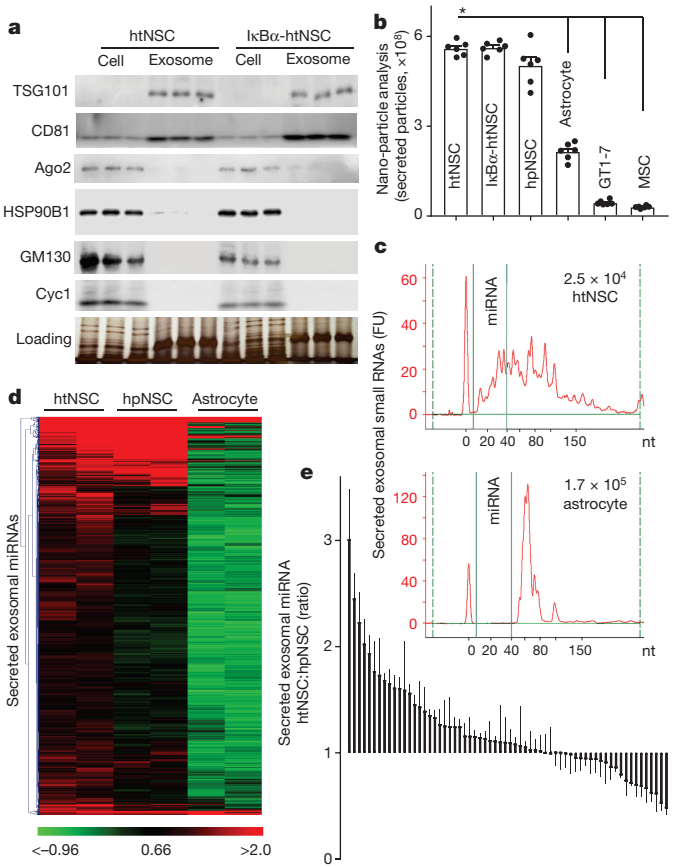

Figure 4 | Exosomes and exosomal miRNAs secreted by htNSCs. **a**–**e**, Secreted exosomes isolated from the same number of indicated cells were assessed by western blotting for indicated exosomal or non-exosomal markers (**a**) and analyses using Nanoparticle tracking (**b**), small RNA bio-analyser (**c**) and miRNA analysis via microarray chip analysis (**d**) and qPCR (**e**). FU, fluorescence unit. **e**, Secreted exosomal miRNA species identified to be abundantly released by htNSCs were compared to their release from hippocampal NSCs (hpNSCs). For details in Supplementary Data 1, 2 (**d**, **e**). $*P < 10^{-4}$; one-way ANOVA with Tukey's test (**b**); $n = 3$ (**a**) or $n = 6$ (**b**) independent samples per group or 2–3 independent experiments (**a**, **c**–**e**). Data are mean ± s.e.m.

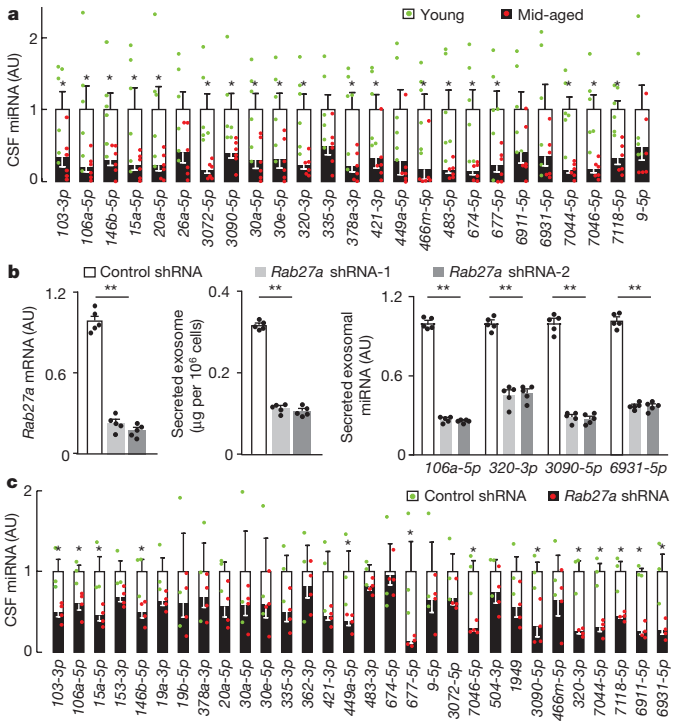

Figure 5 | Contribution of htNSCs to exosomal miRNAs in the CSF. **a**, Exosomal miRNAs in the same volume of CSF from young or mid-aged C57BL/6 mice (each miRNA in the young group was normalized to 1). **b**, Cultured htNSCs were co-infected with Cre-dependent *Rab27a* shRNA (shRNA-1 or -2) or control scramble shRNA lentiviruses with Sox2-promoter-driven Cre lentiviruses. *Rab27a* mRNA expression, amount of secreted exosomes in the medium and the expression of indicated miRNAs in purified secreted exosomes were analysed. **c**, C57BL/6 mice (4 months old) were injected in the hypothalamic third ventricle with Sox2-promoter-driven Cre lentiviruses and Cre-dependent Rab27a shRNA or control scramble shRNA lentiviruses. CSF samples collected at one week after injection were analysed for miRNAs. $*P < 0.05$, $**P < 0.01$; two-tailed Student's *t*-test (**a**, **c**), one-way ANOVA with Tukey's test (**b**); $n = 6$ independent samples per group (**a**), $n = 3$ (Control-shRNA) or 4 (Rab27a-shRNA) independent samples per group (**c**), each sample was a pool of 3–4 mice (**a**, **c**), and $n = 5$ independent samples per group (**b**). Data are mean ± s.e.m.

Despite the fact that hippocampal NSCs also greatly produced exosomes, the amount of exosomal miRNA from these cells was lower and the pattern of miRNA secretion was different to htNSCs (Fig. 4e). Therefore, htNSCs have a notable endocrine function of secreting exosomal miRNAs.

Contribution of htNSCs to exosomal miRNAs in the brain

Using information from miRNA microarray affymetrix chips (Fig. 4d), we analysed miRNAs in the cerebrospinal fluid (CSF) samples collected from young or mid-aged mice. Focusing on miRNA species that are abundantly produced by htNSCs, we found that over 20 miRNA species were substantially decreased in the CSF of mid-aged mice (Fig. 5a). To test whether the reduction in these miRNAs in the CSF of mid-aged mice could be due to ageing-associated loss of htNSCs, we designed an experiment in which exosomal secretion of htNSCs was genetically inhibited. To do so, we created a lentivirus containing a Cre-dependent shRNA against Rab27a, a key molecule for the function of exosomal secretion. Through co-infection with a Sox2-promoter-driven Cre lentivirus, and using two independent shRNA sequences against *Rab27a* mRNA, we confirmed that this approach led to reduced secretion of exosomal miRNAs in cultured htNSCs (Fig. 5b). In addition, we analysed a list of growth factors and cytokines and found that *Rab27a* shRNA did not affect the secretion of a majority of these peptide hormones from htNSCs (Extended Data Fig. 7). This inhibitory effect on exosomal release by *Rab27a* shRNA was not a result of cell loss, as *Rab27a* shRNA did not immediately affect the survival or proliferation of these cultured cells (Extended Data Fig. 8a, b). Therefore, we injected the Sox2-Cre lentivirus together with *Rab27a* shRNA or a control shRNA lentivirus into the hypothalamic third-ventricle of young mice. One week later, CSF samples were examined, showing that *Rab27a* shRNA resulted in decreases in many miRNAs in the CSF (Fig. 5c). We applied this approach to mid-aged mice and analysed ageing-related physiology at six weeks after injection, during which *Rab27a* shRNA did not yet cause a reduction in htNSCs (but it did so over a long duration, such as three months). As shown in Extended Data Figure 8c, mice injected with *Rab27a* shRNA showed impairments in several aspects of physiology, although to a lower extent compared to the models of cell ablation.

Slowdown of ageing by htNSC-derived exosomes

The results above support a role for exosomal secretion from htNSCs for the control of ageing. We decided to focus this work on htNSC-secreted exosomes, although we also predict that neuropeptide secretion by these cells is relevant, especially in the context of our previous study which showed that GnRH is involved in hypothalamic control of ageing[5], and indeed we observed in this work by using immunostaining that some implanted htNSCs became GnRH-positive

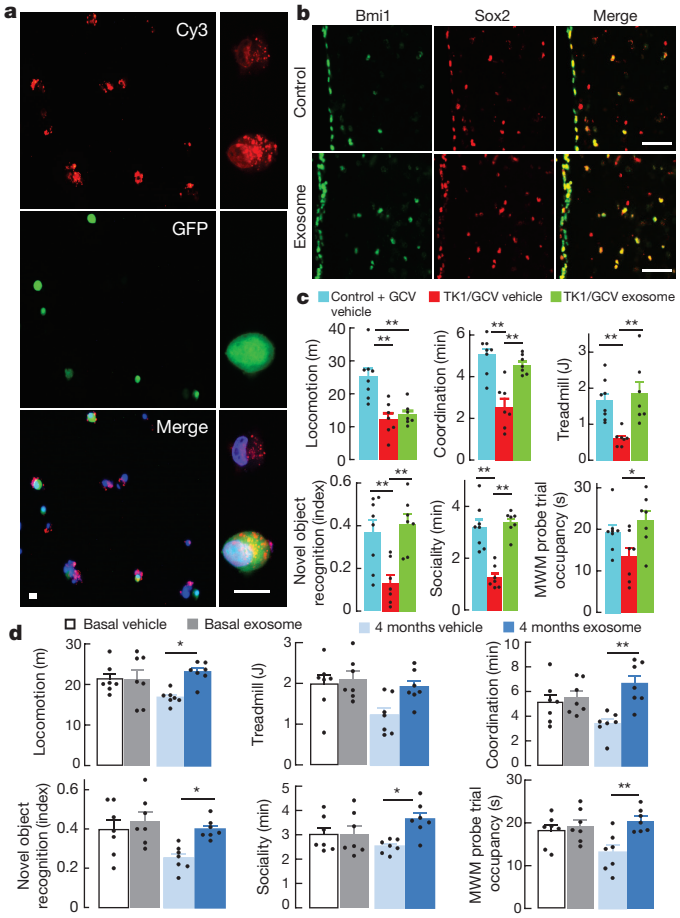

Figure 6 | Slowdown of ageing by treatment of htNSC-derived exosomes. a, GFP-expressing htNSCs transfected with Cy3-labelled miRNAs (106a-5p, 20a-5p and 466m-5p) were co-cultured with htNSCs, which did not contain GFP. Right, high-magnification images of representative GFP^+ and GFP^- cells. Scale bar, 20 μm. **b**, Mid-aged C57BL/6 mice were treated via the hypothalamic third-ventricle cannula with htNSC-derived exosomes or vehicle, three times per week for four months, and examined for Bmi1 and Sox2 expression in the MBH. Scale bar, 50 μm. **c**, Male C57BL/6 mice (15 months old) were bilaterally injected in the MBH with Bmi1-promoter-driven Hsv-TK1 (TK1) or control lentiviruses, followed by GCV or vehicle treatment, and were subsequently treated in the hypothalamic third ventricle with htNSC-derived exosomes (2–3 times per week, three months), and examined for physiology. **d**, Male C57BL/6 mice (16 months old) were treated in the hypothalamic third ventricle with exosomes or vehicle (three times per week, four months) and examined for physiology (**d**). Images represent three independent experiments (**a**, **b**). $*P < 0.05$, $**P < 0.01$; one-way ANOVA with Tukey's post hoc test (**c**, **d**); $n = 8$ mice for control/GCV and vehicle, and $n = 7$ mice for TK1/GCV and vehicle and TK1/GCV and exosome treatments (**c**) and $n = 7$ mice per group (**d**). Data are mean ± s.e.m.

cells (data not shown). Therefore, we tested whether ageing could be slowed down by treatment with htNSC-secreted exosomes that were purified and verified by electron microscopy (Extended Data Fig. 9). First, following the observation that exosomal miRNAs are transferrable among htNSCs (Fig. 6a), we confirmed that central treatment with these exoxomes in mid-aged mice helped maintain htNSCs (Fig. 6b), and that this effect was associated with a reduction in hypothalamic inflammation (Extended Data Fig. 10a). Then, physiological experiments were performed, using an NSC-ablation-induced ageing model and a normal ageing model. To do so, mid-aged mice with TK1/GCV-induced ablation of htNSCs, as described in Figure 2, received a three-month treatment with secreted exosomes purified from cultured htNSCs, which had been derived from newborn mice. Whereas TK1/GCV-induced ablation of NSCs in the control group led to pro-ageing effects, many of these changes were ameliorated by the treatment with exosomes (Fig. 6c and Extended Data Fig. 10b). These anti-ageing effects were not a result of food intake change, as these mice ate similar amounts as the controls. In parallel, we performed an experiment in which mid-aged C57BL/6 mice were treated with exosomes or vehicle for four months. Compared to the vehicle-treated group, which showed many ageing-associated disorders, exosome-treated mice developed these problems to a much lower extent (Fig. 6d and Extended Data Fig. 10c), and these protective effects were also independent of food intake. On the basis of these therapeutic experiments, we show that exosomal miRNAs are important for the role of htNSCs in the control of ageing.

Discussion

We show that loss of htNSCs is an important cause of ageing in the whole body. This understanding aligns with our previous research showing that the hypothalamus has a programmatic role in systemic ageing[5]. The underlying basis could be related to two functions of these cells: endocrine secretion and neurogenesis. Here we report that the modulation of ageing by htNSCs was achieved in a relatively short period, which should not have a major contribution from neurogenesis, while an endocrine function of these cells provided a neurogenesis-independent mechanism. In this context, we show that the anti-ageing effect of htNSCs is partially mediated by exosomal miRNAs secreted from these cells. Therefore, besides the classical endocrine function of the hypothalamus in secreting peptidyl hormones, htNSCs have a new type of endocrine function by secreting exosomal miRNAs. Given this finding, we still predict that neuropeptide secretion by htNSCs, although not addressed in this work, also participates in the regulation of systemic ageing. This is partly because we previously found that GnRH is involved in the hypothalamic control of ageing[5] and we observed here that some implanted htNSCs gave rise to GnRH-expressing cells. Thus, neuropeptide-based endocrine functions of htNSCs and their differentiated offsprings can contribute to the anti-ageing effects of these cells from other perspectives. Despite these outstanding questions, the overall findings in this work support that htNSCs are essential for the control of ageing speed.

Online Content Methods, along with any additional Extended Data display items and Source Data, are available in the online version of the paper; references unique to these sections appear only in the online paper.

Received 3 July 2016; accepted 12 June 2017.
Published online 26 July 2017.

1. Chang, H. C. & Guarente, L. SIRT1 mediates central circadian control in the SCN by a mechanism that decays with aging. *Cell* **153,** 1448–1460 (2013).
2. Fridell, Y. W., Sánchez-Blanco, A., Silvia, B. A. & Helfand, S. L. Targeted expression of the human uncoupling protein 2 (hUCP2) to adult neurons extends life span in the fly. *Cell Metab.* **1,** 145–152 (2005).
3. Alcedo, J. & Kenyon, C. Regulation of *C. elegans* longevity by specific gustatory and olfactory neurons. *Neuron* **41,** 45–55 (2004).
4. Riera, C. E. *et al.* TRPV1 pain receptors regulate longevity and metabolism by neuropeptide signaling. *Cell* **157,** 1023–1036 (2014).
5. Zhang, G. *et al.* Hypothalamic programming of systemic ageing involving IKK-β, NF-κB and GnRH. *Nature* **497,** 211–216 (2013).
6. Satoh, A. *et al.* Sirt1 extends life span and delays aging in mice through the regulation of Nk2 homeobox 1 in the DMH and LH. *Cell Metab.* **18,** 416–430 (2013).
7. Dacks, P. A., Moreno, C. L., Kim, E. S., Marcellino, B. K. & Mobbs, C. V. Role of the hypothalamus in mediating protective effects of dietary restriction during aging. *Front. Neuroendocrinol.* **34,** 95–106 (2013).
8. Sadagurski, M. *et al.* Transient early food restriction leads to hypothalamic changes in the long-lived crowded litter female mice. *Physiol. Rep.* **3,** e12379 (2015).
9. van Praag, H. *et al.* Functional neurogenesis in the adult hippocampus. *Nature* **415,** 1030–1034 (2002).
10. Encinas, J. M. *et al.* Division-coupled astrocytic differentiation and age-related depletion of neural stem cells in the adult hippocampus. *Cell Stem Cell* **8,** 566–579 (2011).
11. Kheirbek, M. A., Klemenhagen, K. C., Sahay, A. & Hen, R. Neurogenesis and generalization: a new approach to stratify and treat anxiety disorders. *Nat. Neurosci.* **15,** 1613–1620 (2012).

12. Merkle, F. T. *et al.* Adult neural stem cells in distinct microdomains generate previously unknown interneuron types. *Nat. Neurosci.* **17,** 207–214 (2014).
13. Sun, Y. *et al.* Neurogenin promotes neurogenesis and inhibits glial differentiation by independent mechanisms. *Cell* **104,** 365–376 (2001).
14. Molofsky, A. V. *et al.* Increasing p16INK4a expression decreases forebrain progenitors and neurogenesis during ageing. *Nature* **443,** 448–452 (2006).
15. Baruch, K. *et al.* Aging-induced type I interferon response at the choroid plexus negatively affects brain function. *Science* **346,** 89–93 (2014).
16. Greenberg, D. A. & Jin, K. Turning neurogenesis up a Notch. *Nat. Med.* **12,** 884–885 (2006).
17. Villeda, S. A. *et al.* The ageing systemic milieu negatively regulates neurogenesis and cognitive function. *Nature* **477,** 90–94 (2011).
18. Sun, F. *et al.* Notch1 signaling modulates neuronal progenitor activity in the subventricular zone in response to aging and focal ischemia. *Aging Cell* **12,** 978–987 (2013).
19. Li, J., Tang, Y. & Cai, D. IKKβ/NF-κB disrupts adult hypothalamic neural stem cells to mediate a neurodegenerative mechanism of dietary obesity and pre-diabetes. *Nat. Cell Biol.* **14,** 999–1012 (2012).
20. Lee, D. A. *et al.* Tanycytes of the hypothalamic median eminence form a diet-responsive neurogenic niche. *Nat. Neurosci.* **15,** 700–702 (2012).
21. McNay, D. E., Briançon, N., Kokoeva, M. V., Maratos-Flier, E. & Flier, J. S. Remodeling of the arcuate nucleus energy-balance circuit is inhibited in obese mice. *J. Clin. Invest.* **122,** 142–152 (2012).
22. Favaro, R. *et al.* Hippocampal development and neural stem cell maintenance require *Sox2*-dependent regulation of *Shh*. *Nat. Neurosci.* **12,** 1248–1256 (2009).
23. Molofsky, A. V. *et al. Bmi-1* dependence distinguishes neural stem cell self-renewal from progenitor proliferation. *Nature* **425,** 962–967 (2003).
24. Strojnik, T., Røsland, G. V., Sakariassen, P. O., Kavalar, R. & Lah, T. Neural stem cell markers, nestin and musashi proteins, in the progression of human glioma: correlation of nestin with prognosis of patient survival. *Surg. Neurol.* **68,** 133–143 (2007).
25. Faiz, M. *et al.* Adult neural stem cells from the subventricular zone give rise to reactive astrocytes in the cortex after stroke. *Cell Stem Cell* **17,** 624–634 (2015).
26. Corti, S. *et al.* Neural stem cells LewisX^{+} CXCR4^{+} modify disease progression in an amyotrophic lateral sclerosis model. *Brain* **130,** 1289–1305 (2007).
27. Buch, T. *et al.* A Cre-inducible diphtheria toxin receptor mediates cell lineage ablation after toxin administration. *Nat. Methods* **2,** 419–426 (2005).
28. Shi, Y. *et al.* MicroRNA regulation of neural stem cells and neurogenesis. *J. Neurosci.* **30,** 14931–14936 (2010).
29. Li, Q. & Gregory, R. I. MicroRNA regulation of stem cell fate. *Cell Stem Cell* **2,** 195–196 (2008).
30. Boon, R. A. *et al.* MicroRNA-34a regulates cardiac ageing and function. *Nature* **495,** 107–110 (2013).

Supplementary Information is available in the online version of the paper.

Acknowledgements This study was supported by NIH R01 DK078750, AG031774, HL113180 and DK099136 (D.C.).

Author Contributions Y.Z., M.S.K., J.Y. and C.H. performed hypothalamic injections and cell implantation; Y.Z. performed immunostaining, cloning, virus production and CSF sampling; M.S.K. performed behavioural experiments and exosome treatment; B.J. performed cell culture, exosome and miRNA characterization; J.Y. performed lifespan follow-up and initial behavioural and miRNA analysis; J.P.Z.-H. performed cell culture and imaging; D.C. conceived the hypothesis, designed and organized the study and wrote the paper.

Author Information Reprints and permissions information is available at www.nature.com/reprints. The authors declare no competing financial interests. Readers are welcome to comment on the online version of the paper. Publisher's note: Springer Nature remains neutral with regard to jurisdictional claims in published maps and institutional affiliations. Correspondence and requests for materials should be addressed to D.C. (dongsheng.cai@einstein.yu.edu).

Reviewer Information *Nature* thanks K. Jin, T. Wyss-Coray and the other anonymous reviewer(s) for their contribution to the peer review of this work.

METHODS

Cell culture. Primary culture of NSCs was performed as described previously[19]. In brief, the hypothalamus and hippocampus were dissected from newborn C57BL/6 mice, cut into small pieces (approximately 1 mm^3), and followed by digestion using TrypLE Express enzyme (Life Technologies) for 30 min at 37 °C. After centrifugation, cells were suspended in NSC medium composed of neurobasal-A (Life Technologies), 0.24% GlutaMAX supplement (Life Technologies), 2% B27 without vitamin A (Life Technologies), 10 ng ml^{-1} EGF (Sigma-Aldrich), 10 ng ml^{-1} bFGF (Life Technologies) and 1% penicillin–streptomycin and seeded in ultralow-adhesion 6-well plates (Corning). One week later, neurospheres were collected by centrifugation and trypsinized with TrypLE Express enzyme into single cells, passaged and maintained in neurosphere culture until experimental use. Hypothalamic astrocytes were isolated from newborn C57BL/6 mice as described previously[31]. In brief, the hypothalamus of newborn mice was dissected, the meninges were removed and cells were dissociated in 0.05% trypsin-EDTA. Mixed cells were cultured at 37 °C in 5% CO_2. Non-adherent cells were removed by changing the medium every two to three days. After 7–10 days, cells were shaken vigorously in an orbital incubator at 0.23*g* at 37 °C for 2 h to detach microglia, then shaken at 0.23*g* at 37 °C overnight to remove oligodendrocytes. Remaining cells were most astrocytes and were trypsinized and reseeded for further culture. HEK293T cells were purchased from ATCC (CRL-3216), and GT1-7 cells were established as previously reported[32]. HEK293T cells, GT1-7 cells and astrocytes were cultured in Dulbecco's modified Eagle medium (DMEM) containing 10% fetal bovine serum and 1% penicillin–streptomycin. Mesenchymal stem cells were isolated from 6–8-week-old C57BL/6 mice as described previously[33]. In brief, bone marrow cells were flushed out of the femurs and tibias, and cultured in DMEM containing 15% fetal bovine serum and 1% penicillin–streptomycin at 37 °C in 5% CO_2. After 3 h, medium was changed to remove non-adherent cells. After 1–2 weeks of culture, cells reached confluence and were passaged for subsequent experiments. All cell lines used in this study were free of microbial (including mycoplasma) contamination and their morphology and growth characteristics were compared to published information to ensure their authenticity.

Plasmids and recombinant lentiviruses. The lentiviral vector of Sox2-promoter-driven Hsv-TK1 and matched control were generated as reported previously[34]. The lentiviral vector of Bmi1-promoter-driven TK1 was generated by replacing the Sox2 promoter with the Bmi1 promoter in the above TK1 plasmid. The lentiviral vector of Sox2-promoter-driven DTR was generated by replacing TK1 cDNA with the coding sequence of simian DTR in the plasmid of Sox2-promoter-driven TK1. Mouse *Rab27a* shRNA and scramble shRNA were constructed using the vector pSico (Addgene). *Rab27a* shRNA-1, GGAGAGGTTTCGTAGCTTA; *Rab27a* shRNA-2, GCTTCTGTTCGACCTGACA; scramble shRNA, ATCTCGCTTGGGCGAGAGT. Plasmids of rAAV2-FLEX-rev-ChR2:tdTomato were purchased from Addgene. Lentiviruses were produced by transfecting viral plasmids and packaging plasmids into HEK293T cells, purified by ultracentrifugation and titrated using the p24 ELISA kit as described previously[32].

Lentiviral infection and miRNA transfection. Lentiviral infection of the cells was performed by adding purified lentiviruses into culture medium for 24 h, before the medium was replaced. Synthetic miRNAs were purchased from Qiagen, including miR-106a-5p, miR-20a-5p and miR-466m-5p, and labelled with Cy3 using the Silencer siRNA labelling kit (Thermo Fisher Scientific, AM1632). Subsequently, 5 μg of miRNA was incubated for 1 h in the dark followed by precipitation of miRNAs by adding ethanol and NaCl. Cy3-labelled miRNAs were transfected into cells using the HiPerFect Transfection Reagent (Qiagen).

Cultured cell immunostaining. Cells were fixed with 4% PFA, blocked with the serum of appropriate species, permeabilized with 0.2% Triton X-100, and incubated with primary antibodies, followed by AlexaFluor 488-, 555- or 633-conjugated secondary antibodies (Invitrogen). Images were captured using a confocal microscope, and counting analysis included at least three coverslips per group and multiple areas per slide on a randomized basis. Primary antibodies included rabbit anti-Sox2 (Millipore, AB5603), rabbit anti-CD81 (Santa Cruz, sc-9158), mouse anti-DTR (Abcam, ab92620), and rabbit anti-Ki67 (Abcam, ab15580) antibodies.

Electron microscopy. Electron microscopy was performed at the St. Giles Foundation Advanced Microscopy Center, Cold Spring Harbour Laboratory. Cells were cultured in laminin-coated 35-mm polystyrene dishes and fixed in 2% glutaraldehyde in 0.1 mol l^{-1} PBS. Cells were post-fixed *in situ* with 1% osmium tetroxide and 1.5% potassium ferrocyanide in distilled water for 1 h. Cells were then dehydrated in a grade series of ethanol and infiltrated with 50% epon-araldite resin (Sigma-Aldrich) for 1 h and then infiltrated for 2 h in 100% resin. Petri dishes were then filled with fresh resin and placed in a 600 °C oven overnight. The polystyrene of the Petri dish was sawn off from the edges of the dish and the disk was plunged repeatedly in liquid nitrogen using differences in thermal expansion to peel off the polystyrene on the bottom of the dish from the epoxy block. The embedded cells were then with the mounted attachment-surface upwards in an ultramicrotome chuck and thin-sectioned at 100 nm. Thin-sections were counterstained with lead citrate and examined in a Hitachi H7500 transmission electron microscope. Representative areas were recorded on Kodak 4489 negative film (Electron Microscopy Sciences) that was then scanned at 2,400 DPI using an Epson V750 Pro scanner.

Exosome isolation and analyses. Secreted exosomes in culture medium were purified by differential centrifugation as described previously[35]. In brief, culture medium was processed by ultracentrifugation at 4 °C overnight to remove particles to generate exosome-free medium. Cells were cultured in exosome-free medium for two days, after which the medium was collected, centrifuged to remove cells, immediately followed by exosome isolation in 4 °C. Exosome-containing medium was centrifuged and filtered to remove debris and particles. Exosomes in the filtered medium were isolated by differential centrifugation. Uncultured medium of the same volume was processed with the same purification procedures and used as a technical control. Isolated exosomes were assessed according to a list of different approaches. (1) Exosomal protein marker immunoblot: exosomal and cellular proteins were loaded and separated by SDS–PAGE, followed by western blotting with primary antibodies, including mouse anti-TSG101 (Santa Cruz, sc-7964), rabbit anti-CD81 (Santa Cruz, sc-9158), rabbit anti-AGO2 (Cell Signaling, 2897), rabbit anti-HSP90B1 (Cell signaling, 2104), mouse anti-GM130 (Santa Cruz, sc-55591), and rabbit anti-Cyc1 (Cell Signaling, 4272). Silver staining was performed using the ProteoSilver Silver Stain Kit (Sigma-Aldrich). (2) Flow cytometry: purified exosomes were incubated with latex beads (Life technologies) for 15 min, adjusted to a final volume, and rotated at room temperature for 2 h, after which glycine was added. After incubation, beads were collected by centrifugation, resuspended and FACS staining was carried out using FITC-conjugated anti-CD81 (ThermoFisher, MA5-17939) antibody. (3) Nanoparticle tracking: purified exosomes were run on NanoSight (Malvern Instruments). These experiments were performed in the Center for Nanotechnology in Drug Delivery at University of North Carolina. (4) Density-gradient ultracentrifugation analysis: isolated exosomes were resuspended in 2.5 M sucrose solution (20 mM HEPES, pH7.4), plated with a continuous sucrose gradient from 2 M to 0.25 M, and ultracentrifuged overnight at 4 °C. Different fractions were collected, each fraction recovered by ultracentrifugation and analysed by immunoblot and real-time PCR. (5) Pull-down assay: anti-CD81 and isotype-control antibodies were coated onto Protein G beads (Life Technologies, 10003D), exosomes were re-suspended in PBS, which contained 3 mg ml^{-1} BSA, and incubated with antibody-coated beads overnight with rotation at 4 °C, and subsequently beads were washed with the same buffer. Isolated exosomes were analysed by real-time PCR. (6) Exosomal total protein and RNA: exosomal total protein concentration was measured by Pierce Coomassie (Bradford) Protein Assay Kit (ThermoFisher). Exosomal total RNAs and small RNAs were purified using the mirVana miRNA Isolation kit (Life Technologies). Exosomal total RNAs were measured using a Qubit assay (ThermoFisher).

Exosomal miRNA analyses. Exosomal miRNAs were analysed according to the following approaches. (1) Exosomal small RNA bioanalyser analysis: exosomal RNAs were run on picoRNA chips or small RNA chips of the Agilent 2100 Bioanalyzer system (Agilent technologies), performed at the Molecular Pathology Platform, Herbert Irving Comprehensive Cancer Center, Columbia University, New York. The exosomal miRNA concentration was calculated according to the instructions provided by Agilent technologies. In brief, the percentage of miRNA in exosomal total RNA was calculated by bioanalyzer picoRNA chips and small RNA chips, and the miRNA concentration was calculated by multiplying percentage of miRNA by the exosomal total RNA measured by Qubit assay (ThermoFisher). (2) miRNA microarray: the miRNA microarray was performed on the GeneChip miRNA 4.0 Array (Affymetrix) at the Albert Einstein College of Medicine Genomics Core using exosomal small RNAs as input. The miRNA pathway analysis was performed using DIANA-mirPath version 3 online software. (3) miRNA quantitative PCR: miRNA was extracted from purified exosomes or the CSF using the mirVana miRNA isolation kit (Invitrogen) or miRNeasy Mini kit (Qiagen). Extracted miRNAs were reverse transcribed to cDNA using the miRNA first-strand cDNA synthesis kit (Invitrogen or Agilent Technologies), and then subjected to real-time PCR with specific primers and SYBR Green PCR Master Mix (Thermo Fisher Scientific).

Secreted growth factor chip array. Cell models of NSCs were cultured in media without EGF and bFGF for two days, and medium was collected and analysed using the Mouse Growth Factor Array (RayBiotech, AAM-GF-2) according to the manufacturer's protocol. Array images were collected and analysed using the LI-COR Odyssey Fc imaging system.

Animal models. C57BL/6 mice were obtained from the Jackson Laboratory and the National Institute of Ageing. AgRP-Cre mice and POMC-Cre mice were maintained on a C57BL/6 background as we have previously reported[32,36]. All mice

were kept in standard, infection-free housing conditions, with 12 h light:12 h dark cycles and 4–5 mice per cage. Strictly pathogen-free quality of the mouse colonies was maintained through quarterly serology, quarterly histopathologic exams and daily veterinarian monitoring of the general health and care of animals. All mice in this study were kept on a standard normal chow diet obtained from LabDiet (5001, 4.07 kcal gram^{-1}). Only male mice were used in this study. All procedures were approved by the Institutional Animal Care and Use Committee of the Albert Einstein College of Medicine.

Hypothalamic lentiviral injection. Purified lentiviruses suspended in 0.2-μl artificial CSF (aCSF, Tocris Bioscience) were injected bilaterally into the MBH using an ultra-precise stereotactic apparatus (David Kopf Instruments) and the coordinates of 1.7 mm posterior to bregma, 5.8 mm below the surface of the skull, and 0.25 mm lateral to the midline of the brain, via a 26-gauge guide cannula and a 33-gauge internal injector (Plastics One) connected to a 5-μl Hamilton syringe and infusion pump (WPI Instruments). Lentiviruses suspended in 0.4-μl aCSF were injected into the hypothalamic third ventricle using the coordinates of 1.7 mm posterior to bregma, 5 mm below the surface of the skull. Guide cannula was implanted into the third ventricle of mice at the coordinate of 1.7 mm posterior to the bregma and 5.0 mm below the surface of skull.

Chemical treatment and cell implantation. Mice with MBH injection of the TK1-expressing lentivirus were treated with GCV (1–10 μg in 0.5 μl aCSF) or vehicle via the pre-implanted third-vehicle cannula, twice per week for the first month (or the experimental duration if less than one month) and then weekly afterwards throughout the experiment. Mice with MBH injection of the DTR-expressing lentivirus were intraperitoneally injected with diphtheria toxin (25 μg per kg body weight in saline) or the vehicle, twice per week for the indicated duration. For the BrdU-tracking experiment, mice were injected with BrdU (1 μg in 0.5 μl aCSF) via the pre-implanted cannula twice per day for one week. Exosome treatment was performed by using exosomes (100 ng protein, purified from cultured htNSCs of newborn mice) three times per week for a duration of 3–4 months as indicated. Cell implantation was performed as described previously[19]. In brief, cultured cells suspended in 0.5 μl PBS were bilaterally injected into the MBH (9,000 cells each MBH side) using the coordinates of 1.7 mm posterior to bregma, 5.8 mm below the surface of the skull, and 0.25 mm lateral to the midline of the brain via a 26-gauge guide cannula and a 33-gauge internal injector connected to a 5-μl Hamilton syringe and infusion pump.

Behavioural tests. All behaviour tests were performed in the behavioural testing room. An Anymaze video-tracking system (Stoelting) equipped with a digital camera connected to a computer was used for the whole course of animal activities in training and experimental sessions of behavioural tests, including the following tests. (1) The grip test (muscle endurance): as described previously[37], each mouse was lifted by the tail and placed on a homemade square grid (1-cm mesh size), the grid was then inverted 30 cm over a soft pad, and the mouse was allowed to hang by paws for 2–6 min according to age conditions. The time that the mouse was able to hang was recorded during a 2-min test period. Three repeats were performed for each mouse with at least 10 min rest between each trial. (2) Rotarod test (coordination): mice were trained on a rotarod (Columbus instruments) that was moving at a constant speed of 6 r.p.m. for 60 s. After a 10-min rest, each mouse was given three trials, during which the rotarod started at 6 r.p.m. and accelerated by 2 r.p.m. per min until 10 min, and there was 30-min rest period between each trial. (3) Treadmill: the treadmill test was performed using a Treadmill Simplex II (Columbus Instruments), which has a capacity of exercising up to six mice simultaneously in individual lanes. Mice were warmed up for protection against running injury and failure before experimental running. For acclimatization to the treadmill, the mouse was placed on the treadmill running at a low speed (6 r.p.m.) for 5 min. The test session started at a speed of 8 r.p.m., and the speed was increased by 2 r.p.m. every min for 10 min. The time at which the mouse retired was recorded. (4) Sociality: using a standard procedure as described[38], social interaction was tested in a grey three-chamber neutral box cage (plexiglas, 60-cm length, 40-cm width, 22-cm height). Before the first session, each mouse was allowed to explore freely for 5 min in the neutral cage to habituate to the testing conditions (adaptation). During the first session (social affiliation), a new mouse (stranger 1) was placed in a wire containment cup that was located in one side chamber. The subject mouse was allowed free access to explore each of the three chambers for 10 min. During the second session (preference), a second new mouse (stranger 2) placed in a wire containment cup was put in the opposite side chamber. The subject mouse freely explored each of the three chambers for 10 min. The time spent in social interaction (sniffing) was recorded. (5) Novel object recognition: the object recognition test was conducted as described[39]. An individual mouse freely explored an open-field box (40 cm length × 40 cm width and × 50 cm height) for 10 min before experimental sessions. During the first session (familiarization session), the mouse was allowed to freely explore two similar objects, and during the second session (test session), one of the two objects was replaced by a novel object for 10 min. The amount of time that the mouse spent exploring each object was recorded. A preference index was calculated using the ratio of the amount of time spent exploring any one of the two objects (including novel one) over the total time spent exploring both objects. (6) The Morris water maze (MWM): the MWM test was performed as described[5]. The water tank was filled with 22–23 °C water, crayola non-toxic paint was added to make opaque and white background, and was located in the centre of a small room with extra-maze cues (various black shapes on a white background). The diameter of the maze was 90 cm and divided into four quadrants (northwest, northeast, southwest and southeast). A circular platform with a diameter of 10 cm was placed 25 cm from the wall of the tank. A mouse was placed in the water, in the same starting location for all trials, and was measured for latency, distance and speed travelled to the platform. Hidden-platform training: mice were first required to swim to and sit on a circular visible platform at 0.5 cm above water level for 10 s. If the mouse could not find the platform within 60 s, it was gently guided to the platform using a glass stirring rod. The mouse was then subjected to four consecutive days of training, consisting of a trial per entry location (entry locations were north, south, east and west) for a total of four trials per day. The platform was made invisible by submerging it 1 cm below the surface of the water. Mice were expected to find the location of the invisible platform, and the following parameters were measured: the latency to reach the platform, distance travelled to reach the platform, path efficiency, time spent in and distance travelled in each quadrant and the total distance and swimming speed. Probe trial: on day 5, the mouse was subjected to a single probe trial, in which the platform was removed and animal was allowed to swim for 60 s. The amount of time spent in all quadrants, the distance and the number of times that the mouse crossed the location of the former platform, as well as the total distance and swimming speed were measured. The learning and memory of mice were indicated positively by occupancy time (the total time spent in the target quadrant) in probe trials.

Tissue immunostaining, CSF collection and histology. Mice under anaesthesia were transcardially perfused with 4% PFA, and then the brains were removed, post-fixed and infiltrated with 20–30% sucrose. For immunostaining, brain sections with a thickness of 20 μm were cut using a cryostat, blocked with the serum of the appropriate species, treated with primary antibodies, including mouse anti-Sox2 (R&D Systems, MAB2018), rabbit anti-Sox2 (Millipore, AB5603), mouse anti-Bmi1 (Abcam, ab14389), mouse anti-Nestin (Millipore, MAB353), mouse anti-BrdU (Cell Signaling, 5292), rabbit anti-Ki67 (Abcam, ab15580), rabbit anti-Hsv-TK1 (Santa Cruz, sc-28038), and mouse anti-GFP (Thermo Fisher Scientific, MA1-952) antibodies, and subsequently incubated with AlexaFluor 488 or 555 secondary antibodies. Technical controls for antibody reaction included using naive IgGs of the appropriate species. DAPI staining of sections was used to reveal all cells. For BrdU staining, tissue sections were pre-treated with 2 N HCl for 20 min at 30 °C, washed, followed by incubation with 0.1 M borate buffer for 10 min at room temperature. Fluorescence images of sections were captured using a confocal microscope. Cells of interest in tissue immunostaining were counted in one out of every 3–6 serial sections of the whole target region or a representative subarea, and then the total number of cells was calculated by multiplication according to these factors (which was predicted to be proportional to the actual total number of cells in a 3-dimenstional hypothalamic region). CSF was collected from anaesthetized mice by penetrating a pulled capillary tube into the cisterna magna through the dura mater, as previously described[40], and the fluid of 3–4 mice was pooled as an individual sample, and the same volume for all samples was used for miRNA analysis. Extra caution was taken to avoid any contamination from the blood or tissue during the procedure of collecting the CSF. For tissue histology, skeletal muscles (quadriceps) and dorsal skin dissected from mice were taken and fixed in 10% neutralized formalin at 4 °C overnight, and subsequently embedded into paraffin. Paraffin sections were then prepared at 5-μm thickness and subjected to haematoxylin and eosin staining.

Optogenetics. According to the established protocol[41], AgRP-Cre and POMC-Cre mice received a hypothalamic third-ventricle injection of Hsv-TK1 lentiviruses and an intra-MBH bilateral injection of 0.2-μl rAAV2-FLEX-rev-ChR2:tdTomato viruses (1×10^{13} genomic copies per ml, produced from Applied Biological Materials Inc.). An Optic/Fluid Cannula (Doric Lenses) was implanted into the hypothalamic third ventricle of mice at the coordinates of 1.7 mm posterior to the bregma and 5 mm below the surface of the skull. Mice received GCV treatment through the implanted cannula. During the experiment, light from a diode laser (450 nm, Doris Lenses) was delivered to the brain via an optic fibre (0.22 NA, 200 μm core; Doric Lenses), as previously described[41], including 20 light pulses (10 ms each) for 1 s (20 Hz) followed by a 3-s break, and the sequence was repeated for 1 h in AgRP-Cre mice and 24 h in POMC-Cre mice. The optogenetic stimulation-induced feeding response was assessed by measuring food intake during various time intervals.

Statistics and reproducibility. The Kolmogorov–Smirnov test was used to analyse for a normal distribution of data. A two-tailed unpaired Student's *t*-test was used for analyses, which involved only two groups for comparison, and an ANOVA and appropriate post hoc test were used for analyses, which involved more than two groups for comparisons. Lifespan curves were analysed with a Kaplan–Meier survival curve and *P* values were obtained using a log-rank (Mantel–Cox) test. Data presented were normally distributed, the data variance among comparable experimental groups was similar, and statistical tests for each figure were justified to be appropriate. Sample sizes were chosen with adequate power based on the literature as well as our previous studies, in general without using statistical methods to predetermine sample size. Animals were randomized into different groups with approximately comparable numbers of animals in each group whenever possible. No samples or data points were arbitrarily excluded from statistical analysis. Experimental performers were generally not blind to group information. Key experiments, including mouse models of htNSC ablation and htNSC implantation and their behavioural analyses; exosomal miRNA experiments, including microarrays, small RNA/miRNA bio-analysis, nanoparticle analysis and qPCR; and mouse CSF sampling and analysis, were all independently repeated with similar observations. All data were presented as mean ± s.e.m., and $P < 0.05$ was considered statistically significant.

Data availability. All Source Data supporting the findings of this study are available in the online version of the paper. Microarray data are also available in the Supplementary Information.

31. Fraczek, L. A., Martin, C. B. & Martin, B. K. c-Jun and c-Fos regulate the complement factor H promoter in murine astrocytes. *Mol. Immunol.* **49,** 201–210 (2011).
32. Zhang, X. *et al.* Hypothalamic IKKβ/NF-κB and ER stress link overnutrition to energy imbalance and obesity. *Cell* **135,** 61–73 (2008).
33. Soleimani, M. & Nadri, S. A protocol for isolation and culture of mesenchymal stem cells from mouse bone marrow. *Nat. Protoc.* **4,** 102–106 (2009).
34. Jin, K., Wang, X., Xie, L., Mao, X. O. & Greenberg, D. A. Transgenic ablation of doublecortin-expressing cells suppresses adult neurogenesis and worsens stroke outcome in mice. *Proc. Natl Acad. Sci. USA* **107,** 7993–7998 (2010).
35. Li, J. *et al.* Exosomes mediate the cell-to-cell transmission of IFN-α-induced antiviral activity. *Nat. Immunol.* **14,** 793–803 (2013).
36. Purkayastha, S., Zhang, G. & Cai, D. Uncoupling the mechanisms of obesity and hypertension by targeting hypothalamic IKK-β and NF-κB. *Nat. Med.* **17,** 883–887 (2011).
37. Fry, C. S. *et al.* Inducible depletion of satellite cells in adult, sedentary mice impairs muscle regenerative capacity without affecting sarcopenia. *Nat. Med.* **21,** 76–80 (2015).
38. Kaidanovich-Beilin, O., Lipina, T., Vukobradovic, I., Roder, J. & Woodgett, J. R. Assessment of social interaction behaviors. *J. Vis. Exp.* (48) 2473 (2011).
39. Leger, M. *et al.* Object recognition test in mice. *Nat. Protoc.* **8,** 2531–2537 (2013).
40. Yan, J. *et al.* Obesity- and aging-induced excess of central transforming growth factor-β potentiates diabetic development via an RNA stress response. *Nat. Med.* **20,** 1001–1008 (2014).
41. Aponte, Y., Atasoy, D. & Sternson, S. M. AGRP neurons are sufficient to orchestrate feeding behavior rapidly and without training. *Nat. Neurosci.* **14,** 351–355 (2011).

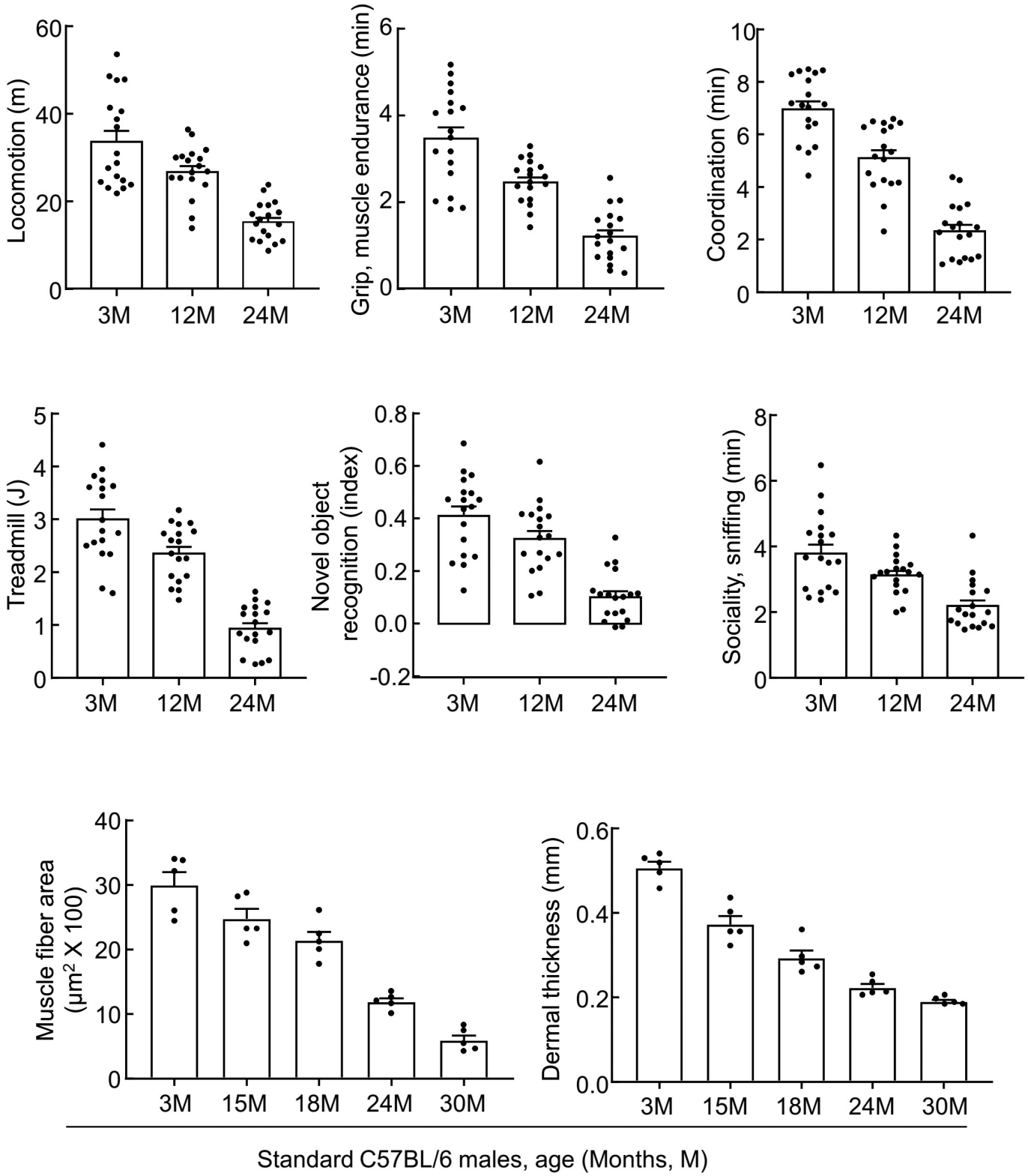

Extended Data Figure 1 | Ageing-related physiology and histology in C57BL/6 mice. Male C57BL/6 mice at indicated ages (months, M) were maintained in standard housing conditions and under standard chow-feeding conditions without any experimental treatment, except for analysis of ageing-related physiological parameters and tissue histology as indicated. $n = 18$ mice per group (behaviours) and $n = 5$ mice per group (histology). Data are mean ± s.e.m.

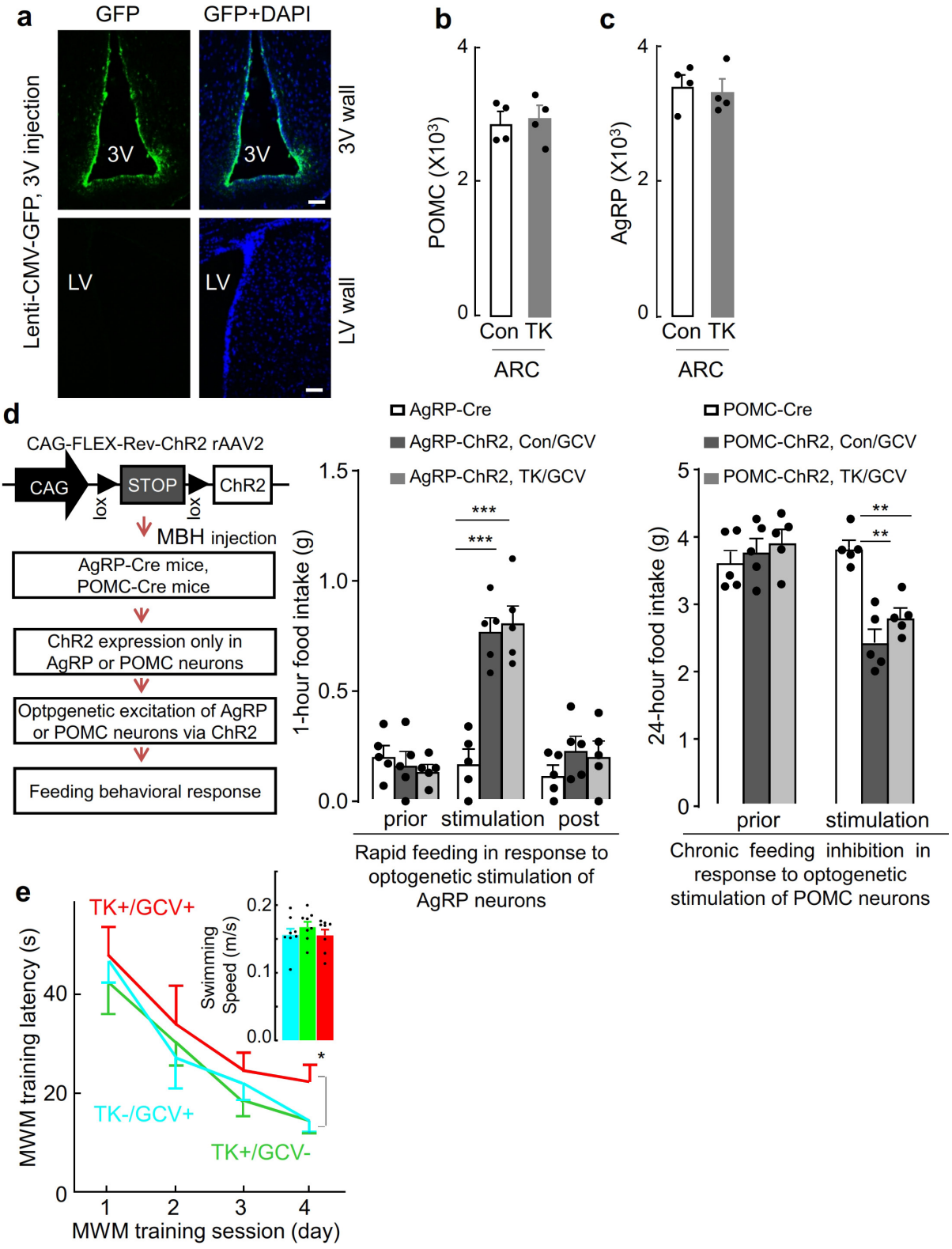

Extended Data Figure 2 | Viral injection and additional information on TK1/GCV model. a, Lentiviruses of CMV-promoter-driven GFP were injected into the hypothalamic third ventricle (3V) of C57BL/6 mice via a pre-implanted cannula. One week after injection, brain sections were made and examined for GFP immunostaining. Scale bars, 50 μm. Images represent four independent experiments. **b**, **c**, AgRP-Cre mice and POMC-Cre mice received an injection in the hypothalamic third ventricle of Hsv-TK1 lentivirus followed by GCV treatment and were examined three months later for the number of AgRP and POMC neurons in the ARC through Cre immunostaining. **d**, AgRP-Cre mice and POMC-Cre mice were injected with rAAV2-FLEX-rev-ChR2:tdTomato virus or vehicle into the ARC, followed by injection of Sox2-promoter-driven Hsv-TK1 lentivirus (TK) or control lentivirus (Con) into the hypothalamic third ventricle. GCV was administrated into the third ventricle twice per week for three weeks. Subsequently these mice were subjected to an optogenetic stimulation-induced feeding response as described in the Methods. Food intake before and after optogenetic stimulation were also measured. **e**, MWM training information for Fig. 1f. $^{**}P < 0.01$, $^{***}P < 0.001$; two-tailed Student's *t*-test (**b**, **c**), one-way ANOVA with Tukey's post hoc test (**d**, **e**); $n = 4$ mice per group (**b**, **c**), $n = 5$ mice per group (**d**) and $n = 8$ mice per group (**e**). Data are mean ± s.e.m.

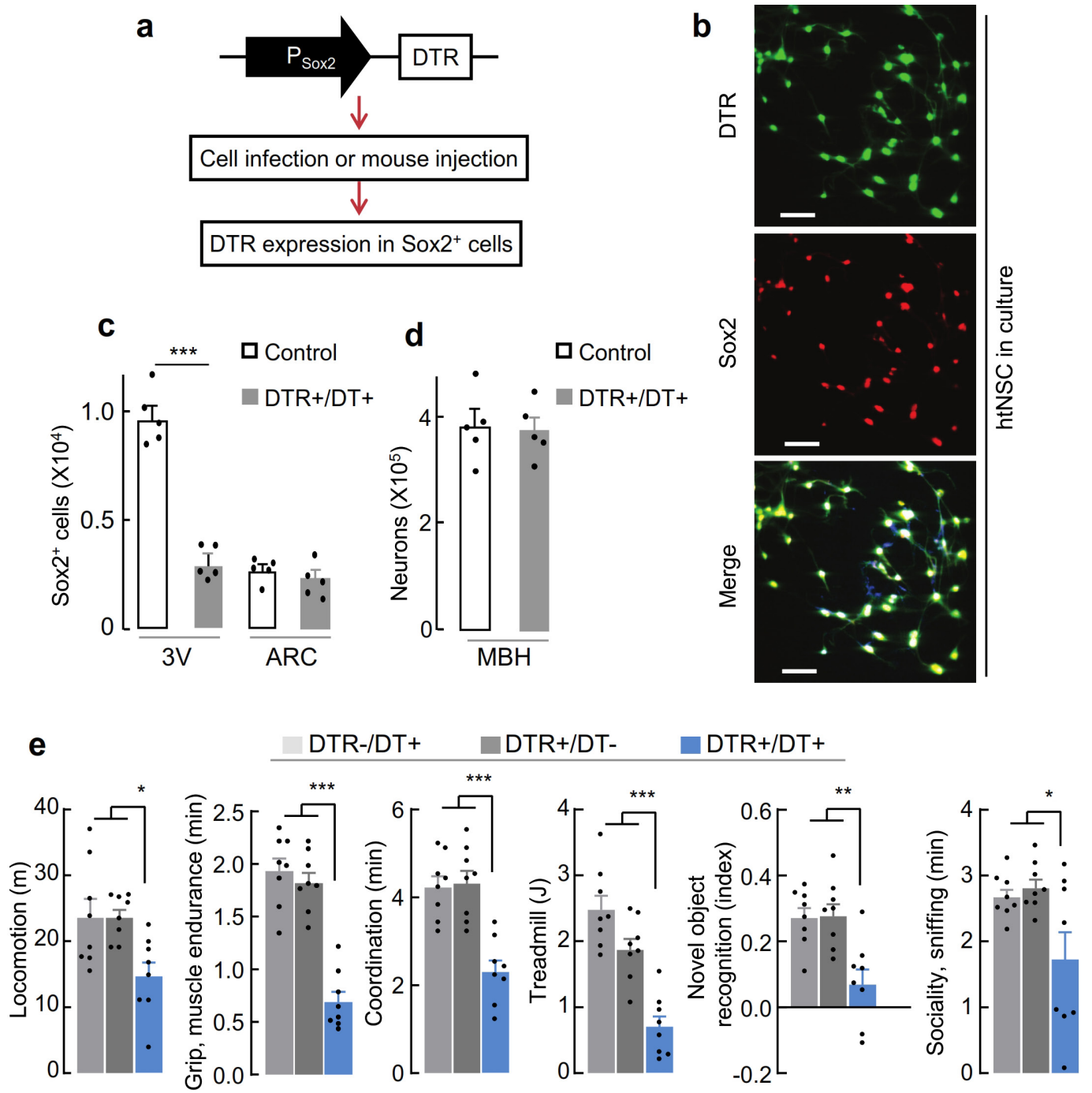

Extended Data Figure 3 | Ablation of htNSCs in hypothalamic third ventricular wall by DTR/diphtheria toxin. Mid-aged male C57BL/6 mice (15 months old) were injected in the hypothalamic third ventricle with Sox2-promoter-directed DTR lentivirus (DTR) or control lentivirus, followed by four-week (twice per week) intraperitoneal injection of diphtheria toxin (DT) or vehicle. **a**, Diagram of lentiviral DTR. **b**, Evaluation of Sox2-promoter-driven DTR lentiviruses in cultured htNSCs by immunostaining of DTR and Sox2. Scale bars, 50 μm. Images represent 3 independent experiments. **c**–**e**, Immunostaining of hypothalamic sections (**c**, **d**) and physiological analyses (**e**) of these mice at three months after viral injection. Control values in **c** and **d** represent similar observations in DTR^{-}/DT^{+} and DTR^{+}/DT^{-} groups. $^{*}P < 0.05$, $^{**}P < 0.01$, $^{***}P < 0.001$; two-tailed Student's *t*-test (**c**, **d**), one-way ANOVA with Tukey's post hoc test (**e**); $n = 5$ mice per group (**c**, **d**) and $n = 8$ mice per group (**e**). Data are mean ± s.e.m.

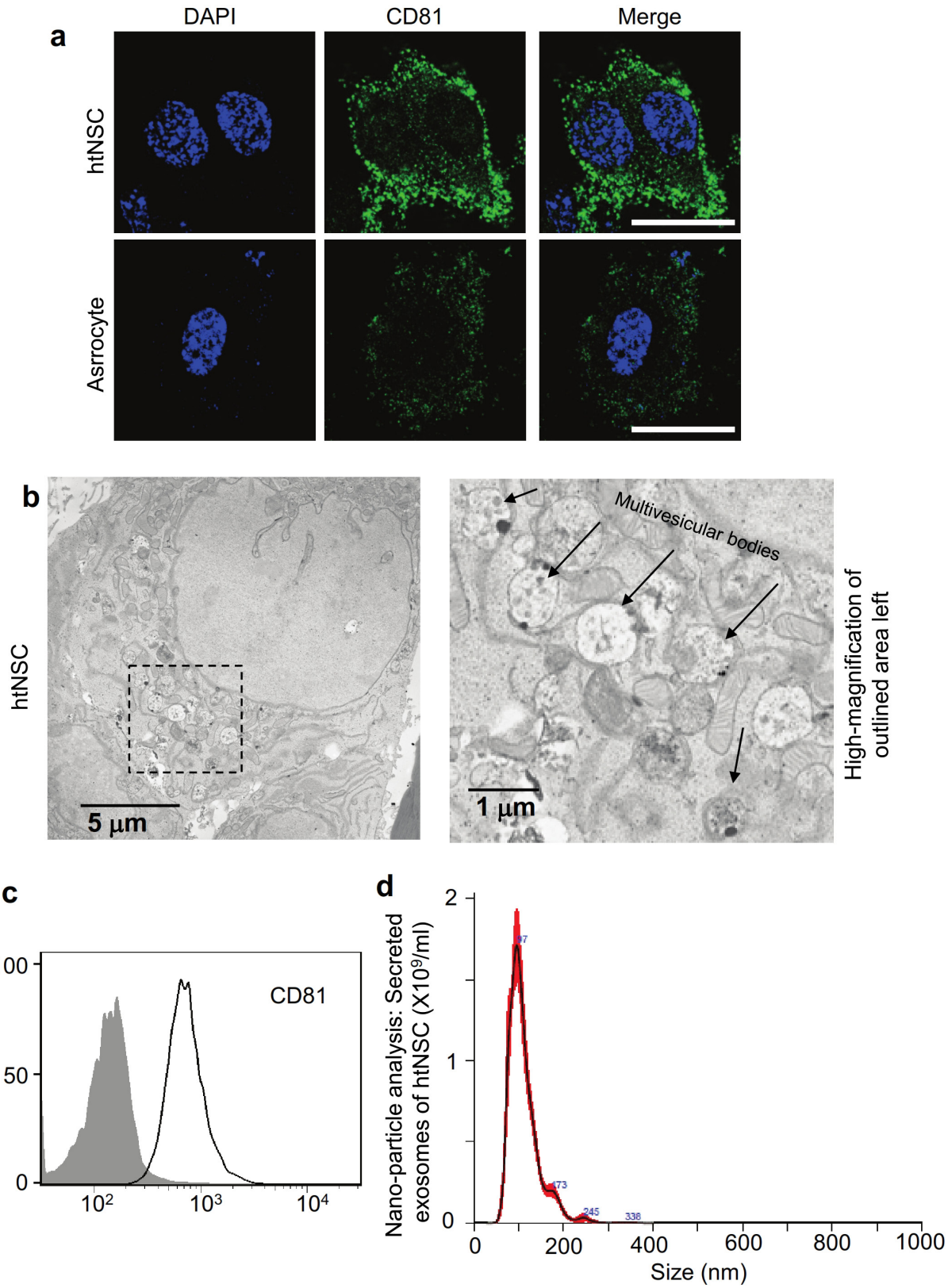

Extended Data Figure 4 | Assessing exosomes secreted by htNSCs. **a**, Immunostaining of CD81 in cultured htNSCs and astrocytes. Scale bars, 10 μm. **b**, Electron microscopic images of htNSCs. Right, high magnification of the outlined area on the left. Black arrows indicate the presence of multivescular bodies. **c**, Flow cytometry analysis of CD81 of htNSC-derived secreted exosomes. Grey area indicates the appropriate isotype control. **d**, Purified exosomes secreted from cultured htNSCs were profiled using nanoparticle analysis. Data represent three independent experiments.

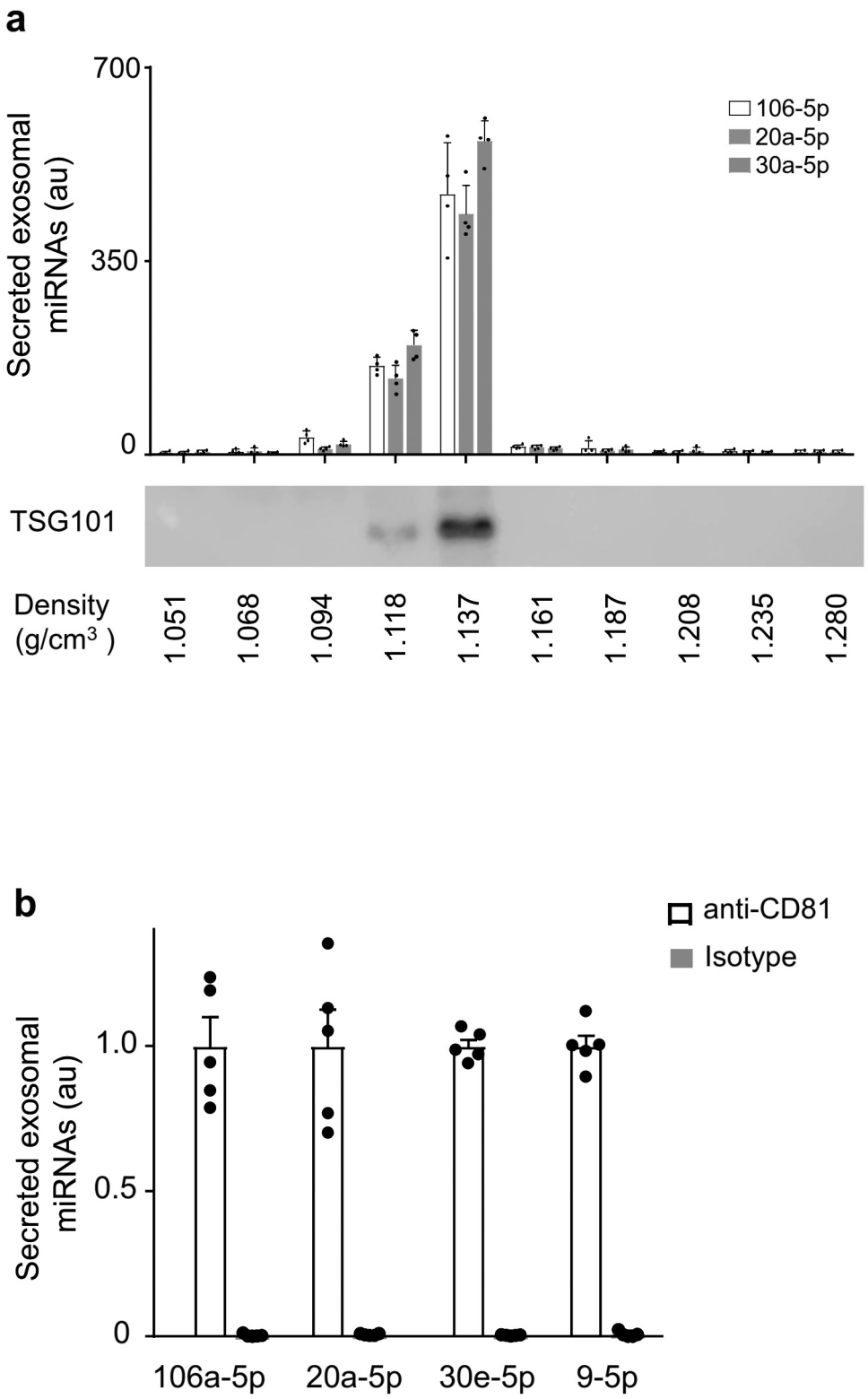

Extended Data Figure 5 | Additional assessments on secreted exosomes from htNSCs. a, Secreted exosomes isolated from htNSCs were subjected to fractioning by density-gradient ultracentrifugation, different fractions were analysed by immunoblotting with anti-TSG101 antibody. **b**, Secreted exosomes isolated from htNSCs were subjected to pull-down by anti-CD81 antibody or appropriate isotype control and then analysed for levels of candidate miRNAs. $n = 4$ independent biological samples per group (**a**) and $n = 5$ independent biological samples per group (**b**). Data are mean ± s.e.m.

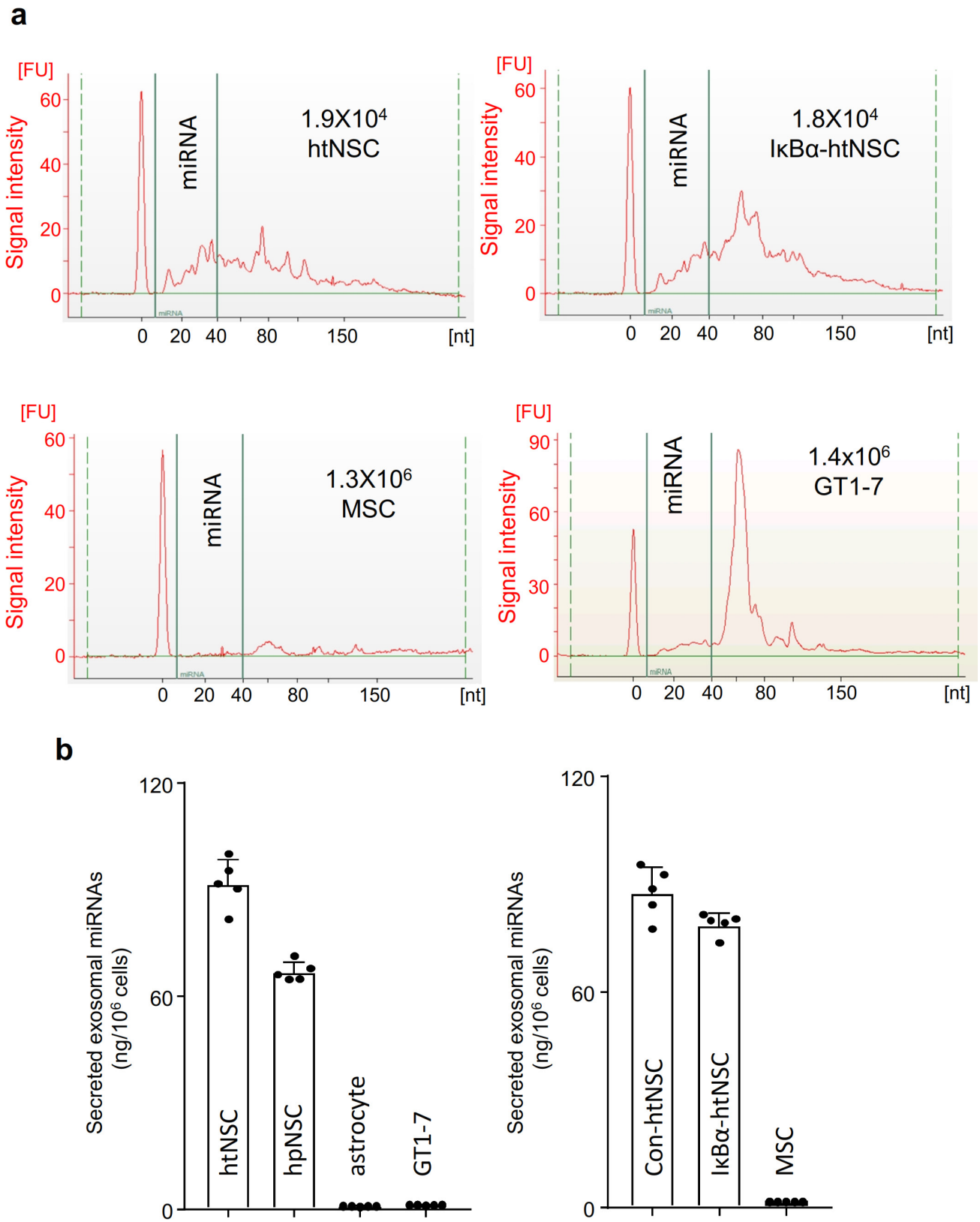

Extended Data Figure 6 | Small RNA bio-analyser assay of secreted exosomes. a, Representative traces of exosomal small RNA and miRNA secreted by htNSCs, IκBα-htNSCs, MSCs and hypothalamic neuronal GT1-7 cells. **b**, Quantification of exosomal miRNAs secreted by indicated cells according to the results from small RNA/miRNA bio-analysis. $n = 5$ independent biological samples per group. Data are mean ± s.e.m.

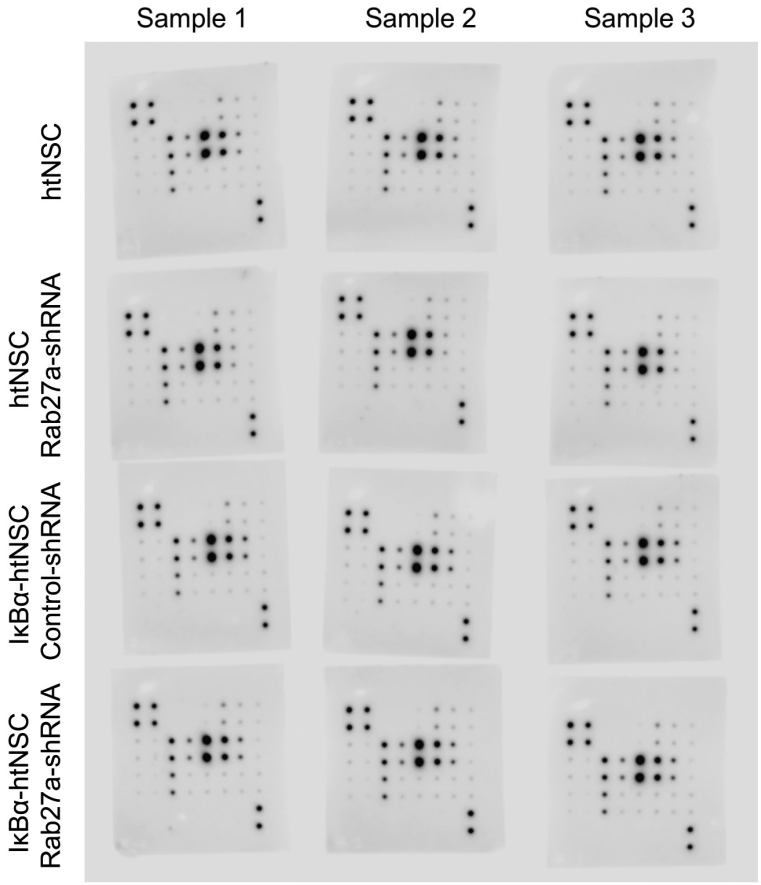

POS	POS	NEG	NEG	Areg	bFGF	EGF	GCSF
POS	POS	NEG	NEG	Areg	bFGF	EGF	GCSF
GM-CSF	HGF	IGF-I	IGF-II	IGFBP-2	IGFBP-3	IGFBP-5	IGFBP-6
GM-CSF	HGF	IGF-I	IGF-II	IGFBP-2	IGFBP-3	IGFBP-5	IGFBP-6
IL-2	IL-7	M-CSF	SCF	VEGF	VEGF-D	VEGF R1	VEGF R3
IL-2	IL-7	M-CSF	SCF	VEGF	VEGF-D	VEGF R1	VEGF R3
Blank							POS
							POS

Growth factor Array Map

POS: Positive standard

NEG: negative control

Extended Data Figure 7 | Growth factors and cytokines secreted by htNSCs. Indicated cells were cultured in medium without EGF and bFGF for 2 days, and the medium was collected and analysed using the Mouse Growth Factor Array for indicated growth factors and cytokines. Array images contain three independent biological samples per cell model (blots on the top and the design of array on the bottom).

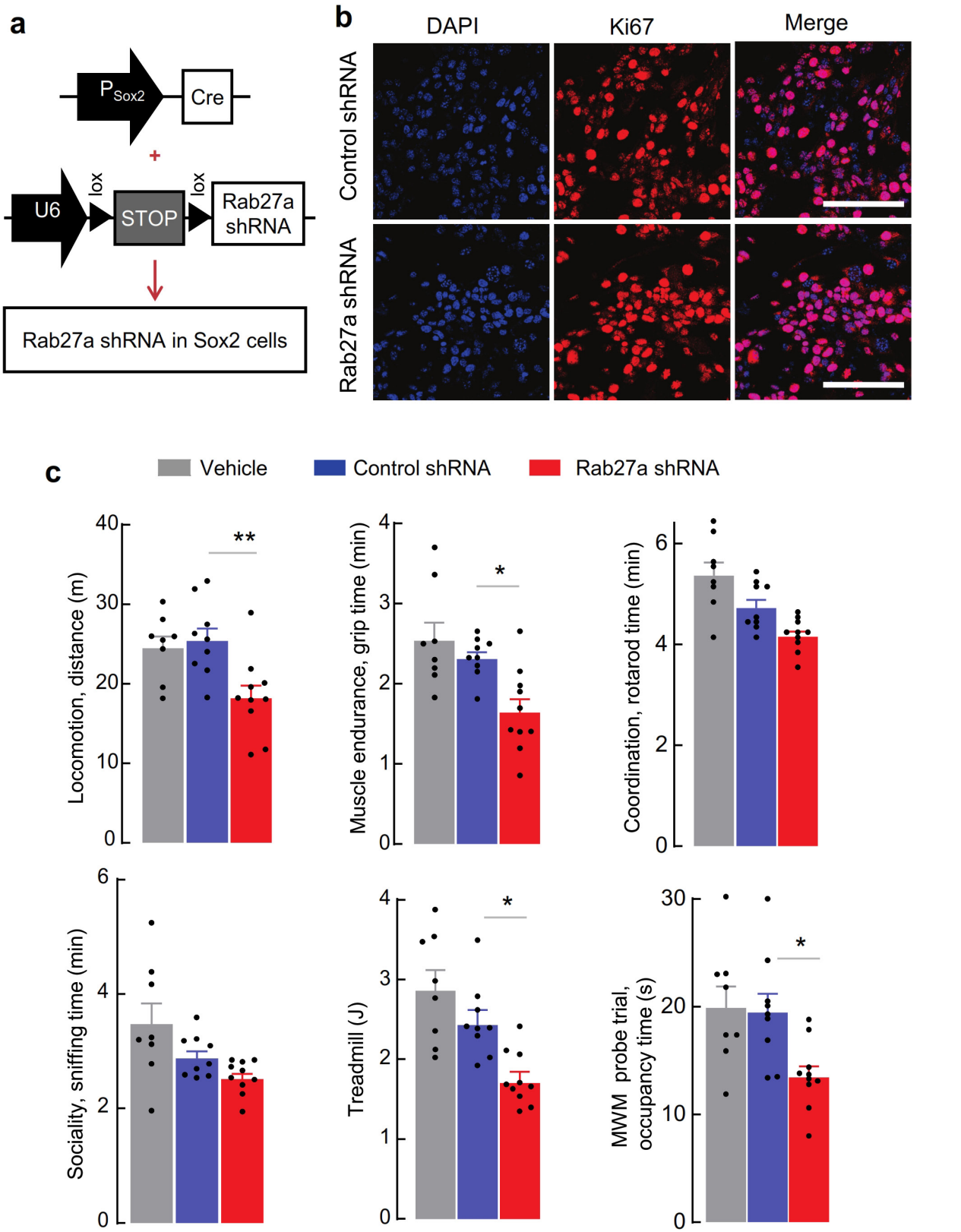

Extended Data Figure 8 | Effects on htNSCs and animal physiology by Rab27a shRNA. a, **b**, Cultured htNSCs were infected with Sox2-promoter-driven Cre lentivirus and Cre-dependent Rab27a shRNA or control scramble shRNA lentivirus (**a**) and examined for Ki67 by immunostaining (**b**) at 2–3 days after viral infection. Scale bars, 60 μm. **c**, C57BL/6 mice (12-month-old males) were injected in the hypothalamic third ventricle with Sox2-promoter-driven Cre lentivirus and Cre-dependent Rab27a shRNA or control scramble shRNA lentivirus or vehicle. Ageing-related physiology was analysed in mice at six weeks after viral injection. $^{*}P < 0.05$, $^{**}P < 0.01$; one-way ANOVA with Tukey's post hoc test (**c**); $n = 8$ mice for vehicle, $n = 9$ mice for control shRNA, $n = 10$ mice for Rab27a shRNA (**c**). Data are mean ± s.e.m.

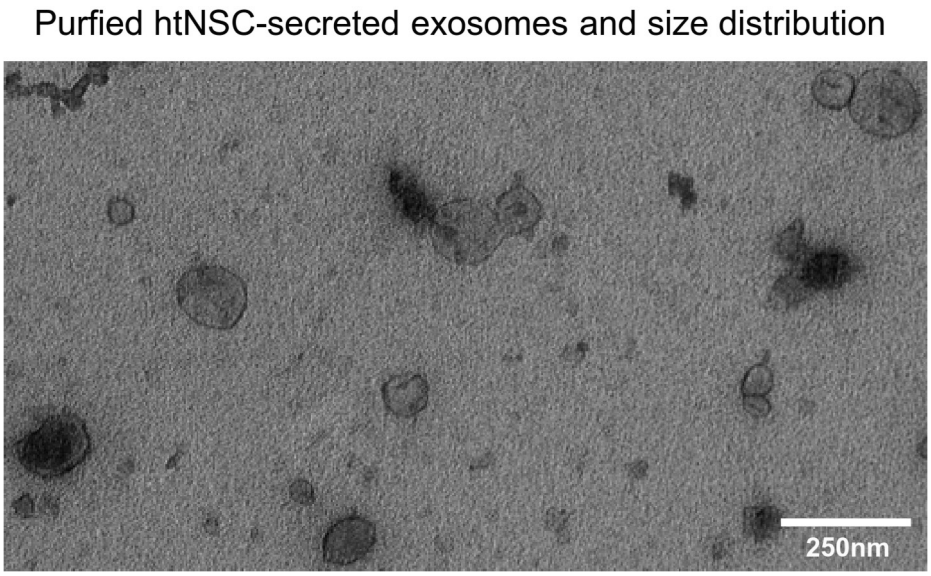

Extended Data Figure 9 | Electron microscopic examination of htNSC-secreted exosomes. Exosomes secreted from cultured htNSCs were obtained and purified using differential ultra-centrifugation and examined for the purity and size distribution by electron microscopy using the protocol detailed in the Methods. Scale bar, 250 nm.

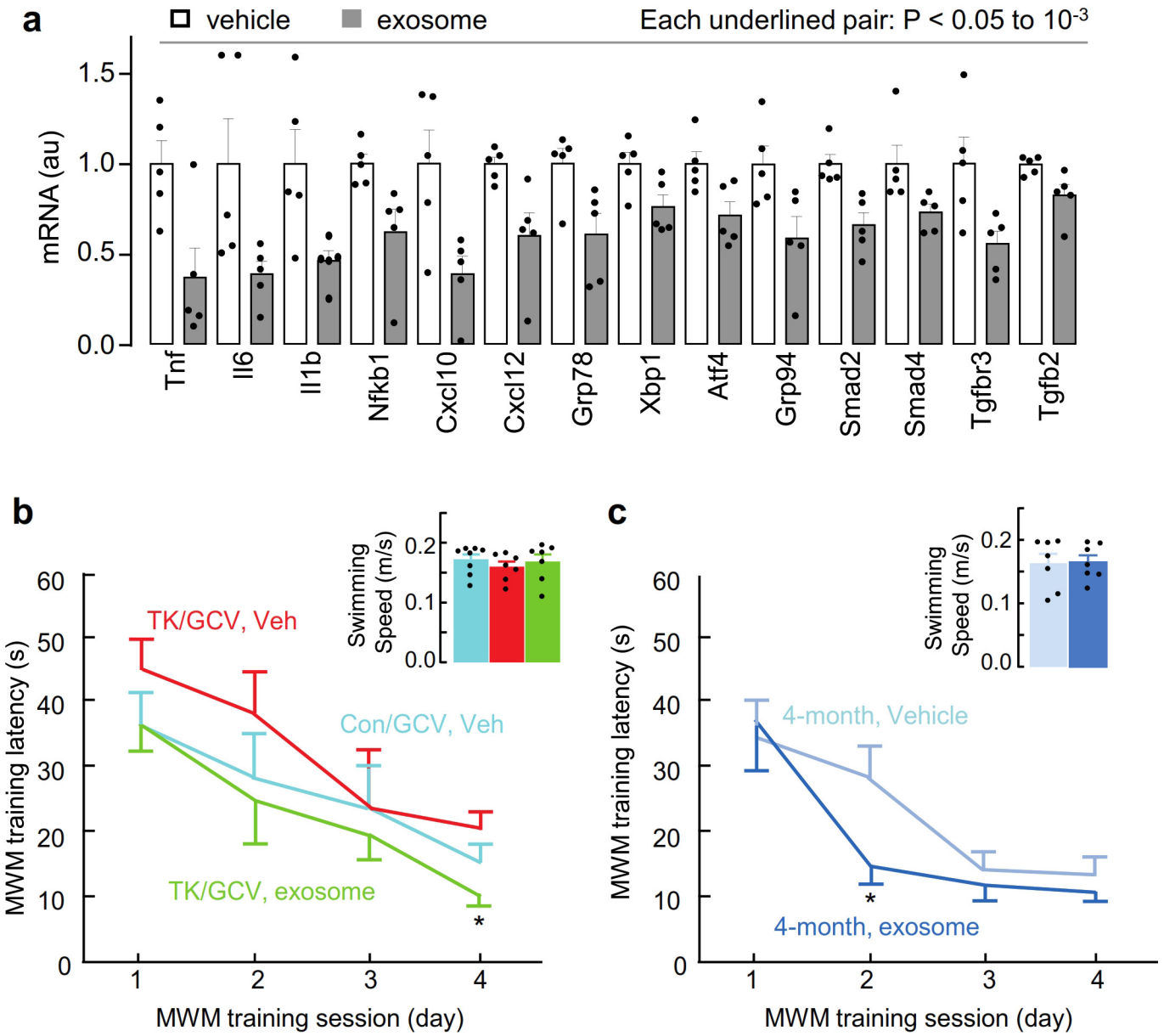

Extended Data Figure 10 | Additional information for the anti-ageing models used in this study. a, C57BL/6 mice (16-month-old males) were treated via hypothalamic third-ventricle cannula with exosomes (100 ng protein, purified from htNSCs) or vehicle, three times per week for four months, and the hypothalamic tissues were dissected and examined for indicated mRNAs. Expression levels of mRNAs are presented in arbitrary units (au), and the value of each species in the control group was normalized to 1. **b**, The training session information for MWM in Fig. 6c. **c**, The training session information for MWM in Fig. 6d. *P < 0.05 (c) or as indicated (**a**); two-tailed Student's *t*-test (**a**) or one-way ANOVA with Tukey's post hoc test (**c**); $n = 5$ mice per group (**a**), $n = 8$ mice for Con/GCV with vehicle, $n = 7$ mice for TK1/GCV with vehicle and TK1/GCV with exosome (**b**), and $n = 7$ mice per group (**c**). Data are mean ± s.e.m.